

Two beams are better than one: Enabling reliable and high throughput mmWave links

Ish Kumar Jain, Raghav Subbaraman, Dinesh Bharadia
University of California, San Diego
{ikjain,rsubbaraman,dineshb}@eng.ucsd.edu

ABSTRACT

Millimeter-wave communication with high throughput and high reliability is poised to be a gamechanger for V2X and VR applications. However, mmWave links are notorious for low reliability since they suffer from frequent outages due to blockage and user mobility. Traditional mmWave systems are hardly reliable for two reasons. First, they create a highly directional link that acts as a single point of failure and cannot be sustained for high user mobility. Second, they follow a ‘reactive’ approach, which reacts after the link has already suffered an outage. We build mmReliable, a reliable mmWave system that implements smart analog beamforming and user tracking to handle environmental vulnerabilities. It creates custom beam patterns with multiple lobes and optimizes their angle, phase, and amplitude to maximize the signal strength at the receiver. Such phase-coherent multi-beam patterns allow the signal to travel along multiple paths and add up constructively at the receiver to improve throughput. Of course, multi-beam links are resilient to occasional blockages of few beams in multi-beam compared to a single-beam system. With user mobility, mmReliable proactively tracks the motion in the background by leveraging continuous channel estimates without affecting the data rates. We implement mmReliable on a 28 GHz testbed with 400 MHz bandwidth and a 64 element phased-array supporting 5G NR waveforms. Rigorous indoor and outdoor experiments demonstrate that mmReliable achieves close to 100% reliability providing 1.5 times better throughput than traditional single-beam systems.

1 INTRODUCTION

5G New Radio (NR) is expected to support cutting edge applications such as V2X, factory automation, autonomous driving, and remote surgery [13]. A key requirement for such applications beyond the high data rate is exceptionally high reliability, defined as the fraction of time during which the link does not suffer an outage [23, 39]. As such, 5G NR utilizes millimeter-wave (mmWave, FR2) frequencies due to abundant bandwidth (400MHz-2GHz) that can provide the high-data-rate compared to traditional sub-6 GHz FR1 (20-100MHz bandwidth) bands [55]. However, unlike its sub-6 GHz counterparts, mmWave uses directional beams to reduce the impact of higher path loss at mmWave frequencies and therefore suffers from severe outage due to blockage and user’s mobility. For instance, a measurement study of 28 GHz network deployment in Chicago [45] shows that human blockages always bring down the link to an outage, which is detrimental for high-reliability applications [39].

Ideally, we would like to create a reliable mmWave link (a link without outage) that achieves high data-rate, is self-reliant, and easy to deploy. However, conventional mmWave design [1] centers on improving the link throughput [48, 69, 83] and coverage [77, 81],

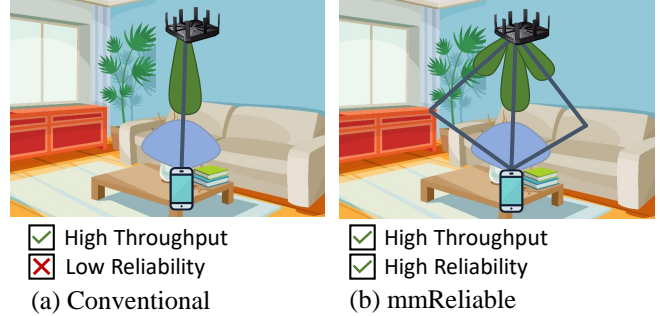


Figure 1: Shows the Conventional mmWave on the left and mmReliable on the right. mmReliable utilizes beam patterns with multiple lobes (*Multi Beam*) to provide high reliability compared to a single-lobe beam pattern.

which inadvertently ends up relegating the reliability requirement. The mmWave base station and the user tediously scan multiple beams in their codebook to establish a directional link through *beam training*. The beam training process is usually *reactive* [15, 20, 21, 34, 38, 68, 84, 84, 86] which kicks in only after a significant degradation in link quality, leading to loss of connectivity and thereof reliability. There are a few *proactive* approaches that act before the link degrades by tracking the user. For this, these proactive approaches either require side-channel information from out-of-band WiFi [46, 66], which has limited accuracy and is limited to indoor environments, or external sensors [32, 74, 76, 80] which are not ubiquitous. All of these approaches make the system difficult to deploy and dependant on external information. In contrast, our goal is to improve system reliability and overall throughput without side-channel or external information.

In this paper, we introduce mmReliable, the first system that achieves high-reliability and high-data-rate mmWave links while being self-reliant (on the mmWave link) and is easy to deploy. mmReliable relies on two novel design principles to achieve the goal of high reliability:

mmReliable’s first design principle is inspired by sub-6 GHz communication, which can deliver high reliability in part by exploiting the multi-path rich environment through omni-directional patterns. The same is not valid for traditional mmWave, which uses a single directional beam along the Line of Sight (LOS) or toward a reflector. mmReliable creates custom beam patterns with multiple directional beams (*multi-beam* for brevity) that are each aligned towards LOS and strong reflected paths, while keeping the Total Radiated Power (TRP) same as a single beam (FCC compliant), as shown in Fig. 1(b). The insight here is that the probability of multiple beams simultaneously facing a blockage is low, reducing the possibility of link outage.

An obvious implication of splitting the single beam to a multi-beam is the loss of EIRP (Equivalent Isotropic Radiated Power) per beam to meet the same TRP constraint. The reduction in per-beam power could reduce the received signal strength and lead to throughput loss at the receiver. At first glance, it seems as if multi-beam trades throughput for reliability while the goal was to improve both. Our insight into breaking this trade-off is based on the observation that the received signal is the sum of multiple copies of the transmitted signal, each for every beam in a multi-beam. If we can ensure the signal adds up in the signal domain constructively, we can increase the signal strength and throughput. Let’s see with an intuitive example, say a mmWave channel consisting of two paths and two-beam are aligned along those two-channel paths. For simplicity, assume the path loss is unity for each path, and the phase of each path is the same. The transmitter splits a total power of a^2 into two beams with power $a^2/2$ on each beam, i.e., amplitude $a/\sqrt{2}$ on each beam while the receiver receives it. Our constructive combining leads to the total amplitude of the received signal $a/\sqrt{2} + a/\sqrt{2} = \sqrt{2}a$, which upon converting to SNR (signal-to-noise ratio) is proportional to $2a^2$. A single-beam link does not exploit the second path and would provide an SNR proportional to a^2 , which is 3 dB lower compared to a multi-beam case. In summary, we can infer that the throughput gain is obtained by harnessing a multi-path environment without increasing the total transmit power.

In the above simple example, we assumed a strong multi-path channel with similar gain as the direct path and aligned phase with the direct path at the receiver. However, real-world channels pose many challenges for multi-beam. They are complex with multi-paths that are weak and have phase value that doesn’t align with the direct path. We develop novel analog beamforming techniques that optimize per-beam phase and power control in a multi-beam to enable constructive combining. We mathematically show that our multi-beam patterns with optimized phase and amplitude are optimal and maximizes the SNR for a given wireless channel. The second challenge for multi-beam is to estimate the phase, attenuation, and angle of each channel path required to generate phase-coherent multi-beam patterns. mmReliable develops a beam probing mechanism to estimate the channel parameters. It exploits the mmWave channel sparsity [17, 45, 54, 56, 68] to keep the probing overhead low. Finally, creating a multi-beam pattern in hardware poses an additional challenge due to hardware imperfections and limited resolution of phased arrays. mmReliable takes advantage of recent advances [36, 59, 62] in antenna design for 28 GHz and shows that the per-antenna analog phase and amplitude control can create efficient multi-beam patterns in our testbed.

mmReliable’s second design principle for reliability is to be *proactive* instead of reactive to blockage and user mobility. mmReliable’s approach is to track the effects of mobility or blockage per-beam in the background by simply leveraging passive measurements of the mmWave received signal, making mmReliable self-reliant. mmReliable uses a tracking algorithm to periodically re-align each beam of the multi-beam and adjust their phase and amplitude, even when there is no significant link degradation. For example, in the blockage case, mmReliable reduces the power along the blocked beam long before the link is degraded, thus increasing

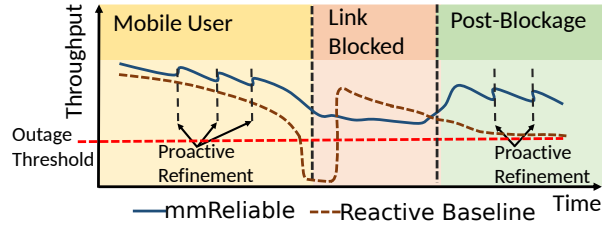


Figure 2: Shows mmReliable tracks the user mobility and proactively refines the multi-beam patterns. It shows the mmReliable link performs well even without beam training overhead. In contrast, the reactive framework performs beam training to recover a dead link.

the power along the unblocked beam and maintaining the link. Similarly, in the case of user mobility, it continually re-aligns the beam directed towards the user. Therefore, mmReliable prevents links from falling into outages, as demonstrated through a prototype in Figure 2.

On a practical system, per beam tracking has to be performed even with user mobility and blockage. mmReliable, therefore, needs to identify whether a particular perturbation in the received signal is due to blockage or user movement. mmReliable leverages received amplitude per beam to make this distinction. The challenge is that the received signal is a combination of all beams in the multi-beam due to a single receiver chain on the receiver (analog beamforming). A naive approach could be to use the received signal to measure the channel in time-domain and use the separation of different beams in time-of-flight to identify amplitude corresponding to each beam. However, the multiple beams can often have very close times-of-flight (ToF) and cannot be resolved even with the high-sampling rate of mmWave (2.5 ns resolution with 400 MHz). To accurately determine amplitude per beam, mmReliable builds a super-resolution algorithm that leverages the relative time-of-flight information (between beams). mmReliable’s insight is that the relative time-of-flight remains constant across multiple packets between beams, and mmReliable uses this insight to learn their amplitudes. Furthermore, the relative ToFs are easily acquired during the initial standard beam training phase, requiring no protocol changes to achieve the tracking algorithm.

Evaluation: We demonstrate mmReliable on a first-of-its-kind software-defined 5G NR testbed on 28 GHz mmWave bands with 64 element phased array, which can support channels of up to 400 MHz. We deploy mmReliable in various indoor and outdoor scenarios and evaluate its performance. Our evaluation shows that in scenarios where user movement and blockage co-occur, mmReliable has a reliability close to 100% while maintaining an average throughput of 1.5 bits/sec/Hz as compared to the single-beam reactive baseline which has a reliability of 65% and on-average throughput of 1 bits/sec/Hz. The throughput-reliability product is improved by 2.3x compared to best reactive baseline.

2 BACKGROUND AND MOTIVATION

This section will provide a brief background on mmWave 5G NR waveform and how mmReliable leverages the waveform structure to establish a reliable and high throughput link. We’ll also explain why traditional single-beam systems suffer from low reliability.

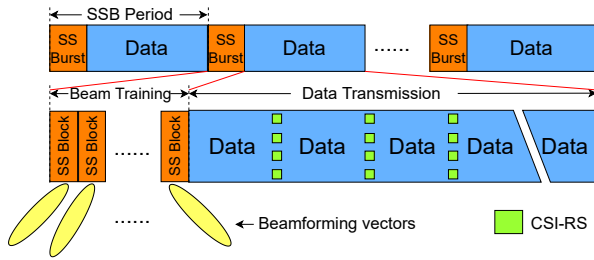


Figure 3: 5G NR downlink waveform uses SSB for beam training and CSI-RS for proactive beam refinement.

We define link reliability as the fraction of time when the link is available for communication. This fraction is vis-a-vis the total time the link is not in outage (due to natural effects) or in beam training, and therefore unavailable for communication.

$$\text{Reliability} = 1 - \text{Prob}(\text{Outage}) \quad (1)$$

where the probability of outage can be practically computed as the fraction of duration when the data rates are below a certain threshold.

2.1 Why 5G mmWave suffers from low throughput and reliability?

The traditional mmWave system establishes a single directional link with the UE (user equipment) to combat high path loss at mmWave frequencies. Though this approach is simple and works in practice, it is not optimal for establishing a high throughput high-reliability link for two main reasons. First, a single-beam acts as a single point of failure with link blockage. A blockage occurs due to higher penetration losses and reduced diffraction around entities like walls and people, penalizing Signal to Noise Ratio (SNR) by 20 to 30 dB [44]. Thus, a single-beam link can bring down a link to an outage, limiting the reliability of such a system. Second, a single directional beam does not exploit the channel-dependent beamforming [16, 38, 48, 58], which are shown to maximize link throughput.

Another important reason for low reliability is how the traditional system reacts to user mobility. Mobility due to rotation (VR headset in motion, rotary industry parts) or translation (walking, moving vehicle) adversely affects the established links by causing misalignment between transmit and receive beams. These effects cause significant throughput loss leading to frequent communication outages. Traditional in-band solutions use a pre-computed back-up beam hoping that they are still available and not blocked. An alternate solution is to gradually widen the beam with user mobility [29] which trade-offs throughput for reliability while still prone to outages. Past work that tracks a mobile user [83] ignores the misalignment due to device rotation.

2.2 Primer mmWave 5G NR beam management

The high overhead in reviving a dead link with vanilla 5G NR (FR2: 24.25 GHz to 52.6 GHz) can further exacerbate the impact of an outage. 5G NR periodically performs the beam training using Synchronization Signal Block (SSB) to recover the directional link, as shown in Figure 3. Multiple SSBs form an SS-Burst, which takes

5 ms of channel air time to probe up to 64 beam directions. The user equipment (UE) will measure the received SSB and report measurement [11, TS 38.215] to gNB (5G NR base station) so gNB will know the best beam. SS-Bursts are transmitted periodically with a transmission period that varies from 5ms to 160ms (default periodicity is 20 ms) [11, TS 38.311]. A link in outage has to wait until the next beam training is performed. Moreover, in scenarios with frequent blockages and high user mobility, the beam scan periodicity is high, which eats up precious communication time. For instance, the default 20 ms periodicity of a 5 ms beam training phase causes 25% probing overhead [30]. A vast literature focuses on reducing the beam training duration [15, 20, 21, 34, 38, 68, 84, 84, 86], but the high periodicity of SSB in mobile scenarios would still keep the overhead high.

2.3 Motivation for Multi-beam

We leverage the 5G NR waveform structure to enable reliable and high throughput links with low overhead. Instead of focussing on initial beam training, mmReliable focuses on proactively maintaining a link during the data communication through multi-beam constructive combining and user tracking. It leverages the Channel Status Information Reference Signal (CSI-RS) in 5G NR, which provides the knowledge of propagation channel [11, TS 38.215] and can be used for beam refinement. CSI-RS can be transmitted periodically or aperiodically, and if periodically sent, its period varies from 4 slots to 640 slots, which is 0.5 ms to 80 ms. One CSI-RS only occupies one symbol ($8.93\mu\text{s}$) in the slot and only a few frequency subcarriers [11, TS 38.211]. So the overhead caused by CSI-RS is much less compared to SSB. We propose a tractable approach to periodically update the per-beam angle, phase, and amplitude with negligible overhead. Our approach requires only three probes for the 2-beam case and five probes for the 3-beam case, which requires less than 2 ms for three refinement phases. Therefore, mmReliable reduces the periodicity of SSB-based training with low overhead CSI-RS-based beam maintenance. In this way, mmReliable achieves high reliability with low overhead while being compatible with 5G NR standards.

Overview: A multi-beam system is a better choice of analog beamforming than a single beam system even when there are no blockages or user mobility. We show in Section 3 that multi-beams belong to the class of channel-dependent beam patterns, which exploits multipath diversity to improve the signal strength at the receiver and are resilient to blockages. Section 4 provides a design of multi-beam system and Section 5 discusses mmReliable’s proactive response to blockages and user mobility.

3 HOW MULTI-BEAM HELPS WITH THROUGHPUT AND RELIABILITY?

We provide a simple mathematical model to analyze the throughput and reliability performance of the multi-beam link and contrast it with that of a single-beam link. We first discuss a scenario without any blockage and later analyse the impact of blockages on link reliability and throughput.

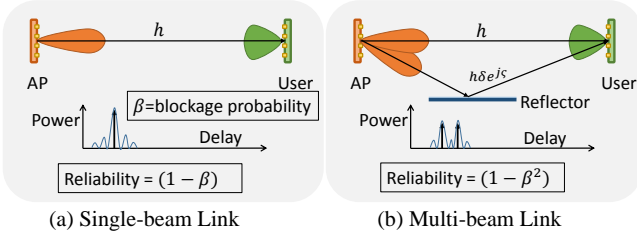


Figure 4: Multi-beam communication enhances the throughput and reliability of a mmWave link through constructive combining optimization.

3.1 Multi-beam vs Single-beam

Here, we evaluate the throughput and reliability of single-beam and multi-beam systems, assuming complete knowledge of the wireless channel. We consider a single-RF chain architecture with an analog phased array. The phased array generates a directional beam pattern (single-beam), which is directed towards the receiver, as shown in Figure 4(a). We assume the single-beam pattern provides an EIRP of P_t . The transmitter transmits a signal x using a single RF chain. The signal experiences a channel attenuation of h along the direct LOS path. For mathematical simplicity, we ignore other paths assuming the high directionality of a single-beam. The received signal would be hx added with the receiver noise. For now, we consider an omnidirectional receiver with the antenna gain of unity and later extend to the directional receiver case. This single-beam link can provide a maximum throughput of [73]

$$C_{sb} = \log_2(1 + |h|^2 P_t / N_r) \text{ bits/s/Hz} \quad (\text{single-beam}) \quad (2)$$

where N_r is the receiver noise power.

Next, we consider a multi-beam link and assume there are two paths (direct path and reflected path) that reach the receiver, as shown in Figure 4(b). We assume that initial beam training has been performed and the two-beams in the multi-beam pattern are perfectly aligned along the two paths. The reflected path suffers large attenuation due to higher path-loss and reflection loss; however, it provides an alternate independent path to the receiver. We model the reflected channel as $h\delta e^{j\xi}$, where δ ($\delta < 1$) is the attenuation factor and ξ is a path-dependent phase shift.

To understand how multi-beam can be helpful for throughput, we first need to know how multi-beam patterns are created. We show that two-lobe beam patterns can be generated as a weighted sum of two equivalent single-lobe patterns, which are oriented towards the direct and reflected path, respectively. Our key insight is to treat multi-beam links similar to a MIMO system with two transmit and one receive antenna, which can deliver high throughput due to transmit diversity [73]. We ask if we can utilize such insight to improve the throughput of a multi-beam link using only an analog phased array without using more than one complex Radio-chains (as in a MIMO system).

Our choice of multi-beam weights is inspired by the concept of transmit beamforming in a MIMO system [73]. We choose the weights such that the two-beams in multi-beam provides a transmit antenna gain proportional to 1 and $\delta e^{-j\xi}$. We normalize the weights

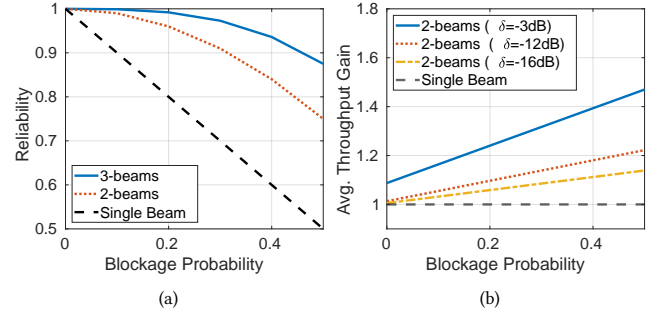


Figure 5: (a) Reliability achieved with blockage probability for mmReliable with 2-beam or 3-beam pattern (b) Throughput gain for mmReliable with a 2-beam pattern w.r.t. single beam for different reflecting surfaces, while all beam patterns meeting the TRP constraint.

to constrain the multi-beam power the same as that of a single-beam. We will derive a formal expression of normalization factor in Section 4, which turns out to be $\frac{1}{\sqrt{1+\delta^2}}$ when the beams in multi-beam are *orthogonal*. The choice of weights ensures that the received signal combine constructively at the receiver and maximize the SNR. Similar to the single-beam case, we assume the receiver is omnidirectional, and the receive antenna gain is unity. The received signal in multi-beam case is

$$y = \left(\frac{1}{\sqrt{1+\delta^2}} h + \frac{\delta e^{j\xi}}{\sqrt{1+\delta^2}} h \delta e^{-j\xi} \right) x + n = (h\sqrt{1+\delta^2})x + n \quad (3)$$

which results in the following throughput [73]

$$C_{mb} = \log_2 \left(1 + (1 + \delta^2) |h|^2 \frac{P_t}{N_r} \right) \quad (\text{multi-beam}) \quad (4)$$

We surprisingly note that the multi-beam throughput is higher compared to that of a single-beam system by a factor of $1+\delta^2$ (which is 2x or 3 dB gain when $\delta = 1$). On a quick glance, the results may seem counter-intuitive since we split power across beams in multi-beam, which results in low EIRP. Despite lower individual EIRP per-beam, multi-beam achieves higher throughput for the same TRP because of the constructive combining of two signals. Intuitively, a multi-beam link enjoys a diversity gain similar to a MIMO system with multiple transmit antennas and one receive antenna. MIMO pre-codes the transmit signal across multiple antennas such that they combine constructively at the receiver. In a multi-beam case, the individual beams are analogous to multiple antennas in a MIMO transmitter. If the phased array can *pre-code* individual beams in a multi-beam, we can get them to combine constructively at the receiver. We discuss our novel analog beamforming method to create such *pre-coded* multi-beam patterns and optimizing them for constructive combining in Section 4.

We now show that multi-beam patterns belongs to the class of channel-dependent beam patterns that are optimal for a given multi-path channel, maximizing the SNR at the receiver.

THEOREM 1. *Multi-beam patterns are equivalent to optimal channel-dependent patterns when the number of beams in multi-beam is the same as the number of channel paths.*

PROOF. We provide the proof in Appendix A \square

| Objects | Metal | Monitor | Wood | Wall |
|------------------|-------|---------|------|------|
| Attenuation (dB) | -3 | -12 | -15 | -16 |

Table 1: Signal attenuation by common materials (path loss plus reflection loss) with respect to the direct path signal.

From (4), we see that the throughput gain of a multi-beam system is dependent on the factor δ^2 , which is the relative attenuation of the reflected path with respect to the direct path. We performed a study of attenuation caused by common reflecting surfaces and verified that 28 GHz attenuation is less severe compared to a 60 GHz link [71]. Shown in Table 1, a metal reflector causes only 3 dB attenuation (including path loss and reflection loss) while other surfaces may create up to 16 dB attenuation. Measurement study for outdoor links [86] also shows that reflected paths from buildings and vehicles are strong with only 5-7 dB attenuation. Note that in certain scenarios when the reflections are weak, multi-beams does not compromise on throughput in normal condition (without blockage) while significantly improving the throughput when one of the paths is blocked (Figure5(b)) as we discuss in the following subsection.

3.2 Impact of Blockage on Link Reliability

We next introduce blockage to our model. Consider a blockage probability β ($0 \leq \beta \leq 1$), which intuitively represents the fraction of time over a period when the link suffered an outage. For simplicity, we assume the beams in our multi-beam set up are blocked independently. Thus, the probability that k beams simultaneously experience an outage is β^k . By definition, the reliability would be $1 - \beta$ for the single-beam case and $1 - \beta^k$, $k \geq 2$ for the multi-beam case. Multi-beam provides higher reliability because it prevents the link to suffer an outage due to blockage, unlike single-beam counterparts [44, 69] as shown in Figure 5(a). Our mathematical result shows that the multi-beam achieves close to 100% reliability for typical blockage probabilities ($< 20\%$).

We next calculate the average throughput gain in the case of blockages. For **single beam** case, the link is sustained only for $1 - \beta$ fraction of time so that the average throughput would be

$$C_{sb}^{avg} = (1 - \beta) * \log_2(1 + |h|^2 P_t / N_r). \quad (5)$$

In contrast, for the case of **multi-beam with 2-lobes**, the average throughput would be obtained by considering whether both beams or only one of the two beams are available:

$$C_{mb}^{avg} = (1 - \beta)^2 \log_2 \left(1 + (1 + \delta^2) |h|^2 \frac{P_t}{N_r} \right) + \beta(1 - \beta) \log_2 \left(1 + |h|^2 \frac{P_t}{N_r} \right) + \beta(1 - \beta) \log_2 \left(1 + \delta^2 |h|^2 \frac{P_t}{N_r} \right) \quad (6)$$

We plot the throughput gain of multi-beam against that of the single beam in Figure 5(b). It shows that multi-beam can achieve up to 1.2 \times higher throughput for 20% blockage instances. So far the analysis assumes an omnidirectional pattern at the user. Our analysis also holds true when the user has a directional pattern. In that case, we propose to use a multi-beam pattern at the user. Interestingly, the user does not need to perform any optimization as only the gNB's phase optimization suffices for constructive combining.

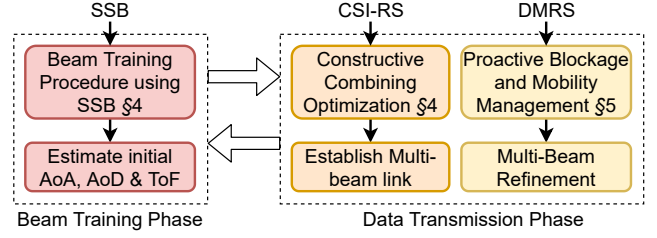


Figure 6: Design Overview: The beam training phase estimates the parameters (AoA, AoD, ToF) required for multi-beam. The data transmission phase establishes and refines the multi-beam providing a proactive response to blockages and user's mobility.

We note that the simplistic example presented above assumes the blockages are independent. In practice, single or multiple blockers might block multiple links at the same time. mmReliable adapts to blockages by tracking its impact on each beam and controlling the power radiated along each blocked or unblocked link. We discuss our blockage detection and power adaptation in Section 5. A simultaneous blockage of all the paths is also not rare for mmWave (e.g., self-blockage by user's hand or body), and it equally affects both the single-beam and multi-beam systems. In such scenarios, the mmWave system may initiate efficient handovers [49, 76] which is out-of-scope of this work.

4 DESIGN OF MULTI-BEAM SYSTEM

4.1 Overview

We present the overall working of mmReliable with the help of a flow-chart in Figure 6. At a high level, mmReliable has two major phases: the **Beam Training Phase (BTP)** and the **Data Transmission Phase (DTP)**. During the BTP, mmReliable leverages the standard exhaustive beam search to estimate some initial parameters such as AoA, AoD, and ToF of each channel path, which is required to establish a multi-beam link. The DTP establishes and periodically refines a multi-beam link through constructive combining optimization. It achieves constructive combining of multi-path signal through two novel contributions: (i) It provides an efficient algorithm and procedure to estimate per-path channel parameters (δ and ζ) required for constructive combining. (ii) It develops a novel analog beamforming method to create phase-coherent multi-beams. The DTP ends when the beam is no longer recoverable by tracking alone (due to accumulated errors in tracking over time) and signals the next BTP. The cycle of BTP and DTP repeats periodically.

4.2 Estimating initial multi-beam parameters

The beam training phase's primary purpose is to scan multiple beams and observe the highest SNR beam pattern. mmReliable leverages this exhaustive scanning process not only to select the highest SNR beam but plots the SNR of each beam with the beam direction and finds all the local maxima and estimates their corresponding directions. The AoA and AoD can be obtained during the transmit scan and received beam scan, respectively. A key challenge, however, is to associate the AoA with the AoD of corresponding reflectors. The mapping of AoA and AoD is non-trivial because of the unknown orientation of transceivers and reflecting surfaces. We

leverage the ToF to solve the association problem. Each reflected path has a unique ToF. When the beam is aligned with some reflector, the strongest signal comes from the reflected path corresponding to that reflector. We take the corresponding path-dependent CIR and estimate the ToF by looking at the highest power index for each path. We performed an $8\times$ upsampling and cosine interpolation of CIR to get the ToF estimates with high precision. We identify the LOS path as the path with the lowest ToF. This way, mmReliable estimates the AoA, AoD, and ToF of each path and associate them with each other. After the initial training, mmReliable creates a multi-lobe beam pattern with constructive combining to establish the directional beam.

4.3 Constructive Combining Optimization

We propose a novel constructive combining optimization algorithm to estimate the relative phase $\hat{\zeta}$ and amplitude $\hat{\delta}$ per beam required for constructive combining. For the 2-beam case, our algorithm requires only two probes to estimate these parameters and in-general $2(K-1)$ probes for K beams. For simplicity, we explain the 2-beam case here. To start with, gNB and the UE create a 2-beam pattern directed towards the AoD and AoA estimates, respectively (Assuming downlink case). The gNB uses two CSI-RS to probe two 2-beam patterns, each with opposite phases of individual beams in the 2-beam as follows:

$$\begin{aligned} \mathbf{p}_1 &= e^{j0}\mathbf{h}_1 + e^{j0}\mathbf{h}_2 = \mathbf{h}_1 + \mathbf{h}_2 \\ \mathbf{p}_2 &= e^{j0}\mathbf{h}_1 + e^{j\pi}\mathbf{h}_2 = \mathbf{h}_1 - \mathbf{h}_2 \end{aligned} \quad (7)$$

where \mathbf{h}_1 and \mathbf{h}_2 is the complex per-path CSI (channel state information) observed by each of two beams across all frequency subcarriers. Using the set of two equations in (7), we estimate the complex per-path channel as $\mathbf{h}_1 = (\mathbf{p}_1 + \mathbf{p}_2)/2$ and $\mathbf{h}_2 = (\mathbf{p}_1 - \mathbf{p}_2)/2$. Note that we inherently cannot estimate $\hat{\zeta}$ that works well for all the subcarriers simultaneously. Our constructive combining approach maximizes the average received signal strength over all frequencies as:

$$\{\hat{\delta}, \hat{\zeta}\} = \arg \max_{\delta, \zeta} \left\| \mathbf{h}_1 + \delta e^{-j\zeta} \mathbf{h}_2 \right\|^2. \quad (8)$$

We solve the above optimization to a closed form expression as:

$$\hat{\delta} e^{j\hat{\zeta}} = -\mathbf{h}_2^H \mathbf{h}_1 / \mathbf{h}_2^H \mathbf{h}_2, \quad (9)$$

which simply reduces to $\hat{\delta} e^{j\hat{\zeta}} = -h_1/h_2$ for a narrowband channel (e.g. in IEEE 802.11ad [1]).

Note that mmReliable requires the full CSI at the receiver for every probe to perform constructive combining. For the 5G NR system, the CSI is readily available from the CSI-RS signal. Even for 802.11ad commercial routers, there is firmware available to extract the CSI [48, 53, 75]. Finally, the optimal phase, amplitude, and angle will change over time as the user moves. We propose to periodically estimate these parameters along with our novel tracking algorithm that we'll discuss in Section 5.

4.4 Creating multi-beam patterns with normalized total radiated power

We devise a simple method to create multi-beam pattern by combining the beamforming weights of respective single beam patterns.

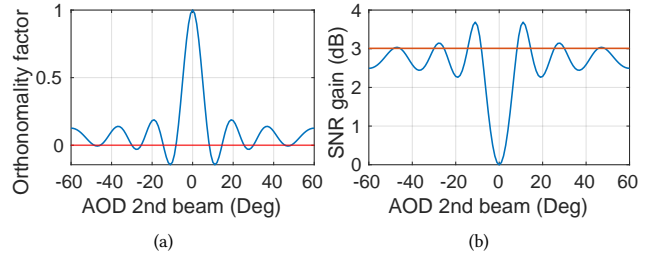


Figure 7: (a) Orthogonality factor is close to zero when beams are separated by more than 12° . (b) The resulting SNR gain approaches 3 dB when beams are orthonormal and stays within ± 0.7 dB, sometimes even higher than 3 dB.

The beamforming weights for a single beam pointing at an angle ϕ_1 is given by

$$\mathbf{w}_{\phi_1} = \frac{1}{\sqrt{N}} [1 e^{j2\pi \frac{d}{\lambda} \sin(\phi_1)} \dots e^{j2\pi(N-1) \frac{d}{\lambda} \sin(\phi_1)}]^T \quad (10)$$

where d is antenna spacing, λ is the carrier wavelength, N is number of antennas. The total radiated power (TRP) is normalized to unity (i.e., $\|\mathbf{w}_{\phi_1}\|^2 = 1$). We design beamforming weights \mathbf{w} for multi-beam with two lobes as follow:

$$\mathbf{w} = \frac{1}{\sqrt{NF}} (\mathbf{w}_{\phi_1} + \hat{\delta} e^{-j\hat{\zeta}} \mathbf{w}_{\phi_2}), \quad (11)$$

where the normalizing factor (NF) is chosen to restrict the TRP to unity as follow

$$\begin{aligned} NF &= \|\mathbf{w}_{\phi_1} + \hat{\delta} e^{-j\hat{\zeta}} \mathbf{w}_{\phi_2}\|^2 \\ &= \|\mathbf{w}_{\phi_1}\|^2 + \hat{\delta}^2 \|\mathbf{w}_{\phi_2}\|^2 + \hat{\delta} e^{-j\hat{\zeta}} \mathbf{w}_{\phi_1}^H \mathbf{w}_{\phi_2} + \hat{\delta} e^{j\hat{\zeta}} \mathbf{w}_{\phi_2}^H \mathbf{w}_{\phi_1} \\ &= 1 + \hat{\delta}^2 + \hat{\delta} \text{Real}(e^{-j\hat{\zeta}} \mathbf{w}_{\phi_1}^H \mathbf{w}_{\phi_2}) \end{aligned} \quad (12)$$

We observe that the NF becomes $1 + \hat{\delta}^2$ when the two single beams are orthonormal (i.e., $\mathbf{w}_{\phi_1}^H \mathbf{w}_{\phi_2} = 0$). We define orthonormality factor as the ratio $\frac{\hat{\delta} \text{Real}(e^{-j\hat{\zeta}} \mathbf{w}_{\phi_1}^H \mathbf{w}_{\phi_2})}{1 + \hat{\delta}^2}$ and show that it indeed is close to zero for a beam separation of half-power beamwidth which is 12° in our system as shown in Figure 7(a). The resulting SNR varies around 3dB (assuming two paths suffers equal channel attenuation) with a maximum variation of ± 0.7 dB shown in Figure 7(b). Intuitively, when the two beams are very close, the channel across two beams becomes correlated due to the wide beam aperture. In the extreme case, when the two beams are merged, it becomes equivalent to a single beam system as understood from Figure 7(b). Thus, the results of (4) hold in general. We emphasize that we used the NF from (12) for normalization (and not the approximate value) to satisfy the TRP constraint in our testbed implementation strictly.

Beam Pattern Quantization: Phase-coherent multi-beam patterns can be generated using minimum 2-bit phase shifters and 1-bit amplitude control (turning antenna on or off) [43, 47, 48] which is available in commercial 802.11ad devices [10, 53] as well as 28 GHz 5G NR [59, 62]. Having higher resolution in phase and amplitude control helps both the single-beam and multi-beam to reduce side-lobe noise. We demonstrate a high-throughput and reliable mmWave link with our state-of-the-art 64 elements phased arrays built in-house [37]. It provides 6 bit of phase control and

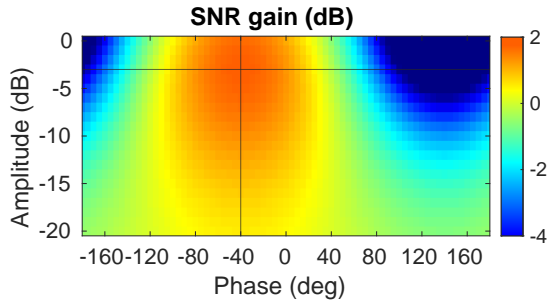


Figure 8: Sensitivity analysis (simulation): SNR gain (dB) of 2-beam w.r.t. single-beam for varying 2nd beam’s phase $\hat{\zeta}$ and amplitude $\hat{\delta}$ in multi-beam. We show for -3 dB weaker multi-path channel, the multi-beam’s highest SNR gain is 1.76 dB which is not very sensitive even for high phase error of $\pm 75^\circ$. However, if the phase error is highest (180°), the SNR drops significantly.

27 dB of gain control per antenna element similar to commercial arrays deployed by Samsung [62] and IBM [59, 61] at 28 GHz¹.

Sensitivity analysis: The SNR gain of multi-beam against single-beam relies on accurate estimation of the per-beam phase and amplitude. We show that the SNR gain has low sensitivity to the estimation error in phase and amplitude. We simulate a two-path channel and set the relative phase and attenuation to -40° and -3 dB, respectively. We vary the relative phase and amplitude of the 2nd beam in a 2-beam pattern (w.r.t. the first beam) and show the 2D plot of SNR gain in Figure 8. The SNR gain is a maximum of 1.76 dB when the 2nd beam phase and amplitude match with the channel phase and attenuation. The SNR gain drops with an increasing mismatch between the beam and channel parameters. We show that multi-beam SNR exceeds the single-beam SNR as long as the estimated phase is within $\pm 75^\circ$. Moreover, the multi-beam outperforms the single-beam system even with a high amplitude estimation error of -20 dB. Thus, the sensitivity to phase and amplitude estimation is low.

Reliability-first principle: At this point, one may wonder that when the multi-path is weak, the multi-beam pattern allocates less power along the reflected-path beam to maximize throughput, which may harm the reliability when the reflected path signal has power below an outage threshold. We solve this challenge by redistributing per-beam amplitudes to satisfy a minimum power constraint along the reflected beam for a fixed total radiated power. Such optimization will ensure high reliability but at a sub-optimal throughput gain. Our insight follows from sensitivity analysis in Figure 8, which shows that even when we do sub-optimal power allocation per beam, e.g., distributing equal power to two beams, the throughput-gain reduces from 1.76 dB to 1.64 dB, which is still better compared to the single-beam case. *Moreover, when the LOS path is not available for a long duration (e.g., persistent static blockage), having two beams at two reflectors with comparable attenuation is significantly better than a single beam from both throughput and reliability points of view.*

¹Verizon, Ericsson, and other commercial vendors deploy the high-resolution 28 GHz phased arrays developed by Samsung, IBM and others [2, 12]

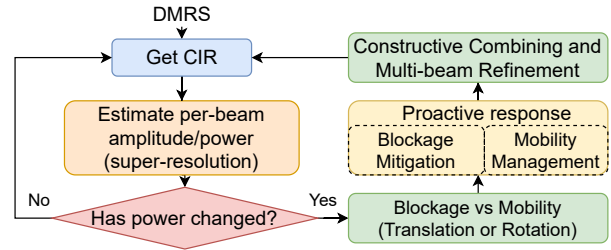


Figure 9: Overview of mmReliable’s proactive response to blockage and mobility. It observes the per-beam amplitude from periodic DMRS channel estimates and classifies whether the user has gone into blockage or mobility. It also classifies mobility into translation or rotation motion and acts differently in each case. Finally, the cycle is concluded by constructive combining optimization and refining of multi-beam patterns at both the gNB and the UE. The cycle is repeated until the link is no longer recoverable by proactive response alone.

5 MMRELIABLE PROACTIVE RESPONSE

In this section, we detail how mmReliable proactively identifies impending blockage and mobility events and responds to them while the communication link is active. An overview is shown in Figure 9. By continuously monitoring the per-beam amplitude (in multi-beam) for changes over time, mmReliable first declares an event as a blockage or mobility. In the case of mobility, it further classifies the user motion into translation or rotation. It recovers the per-beam amplitude at high resolution from the Channel Impulse Response (CIR), obtained from DMRS (Demodulation Reference Signal) channel estimates in 5G NR. We can use this information to refine the beam differently in response to each event.

5.1 Proactive Blockage Mitigation

Mobile blockers interact with the multi-beam system by suddenly occluding one or more active beams. mmReliable analyzes the rate of change of amplitude per beam to detect such events. Empirical evaluation shows that typical blockage events cause per-beam amplitude to degrade by 10 dB in just 10 OFDM symbols. Once a blockage event is detected, mmReliable responds by re-purposing the power on the blocked beam to other unblocked ones. Since there are always multiple beams active, there is no significant impact on link reliability, even if one is blocked. Said differently, the transceiver reduces the number of beams whenever blockage is detected along some paths. It is rare that all paths are blocked simultaneously; nonetheless, in case of a complete outage, the radio can initiate a new phase of beam training to search for other alternate paths or perform an efficient handover [76].

5.2 Proactive User-Mobility Management

If per-beam amplitude changes appreciably, but not quickly, then mmReliable classifies them as caused due to underlying user motion. User motion is difficult to deal with since it is difficult to predict how the user moves without relying on external sensors.

Classification of user motion (translation vs rotation): Our insight here is to decouple complex user motion into one of translation or rotation motion for the small duration of tracking. Since

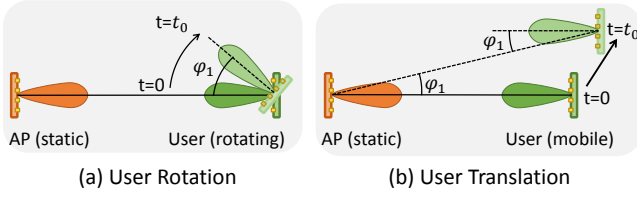


Figure 10: Two cases of user motion: Rotation or Translation for a single beam. Rotation causes misalignment only at the user, while the translation causes misalignment at both the gNB and user.

mmReliable’s tracking works for every OFDM channel estimate, which is as fast as one in every $33\mu\text{s}$ for a 5G NR system. Therefore, practical user motion can be piece-wise decomposed into translation and rotation, significantly simplifying system design.

First, we proactively detect user mobility and classify it into translation and rotation by leveraging per-beam power estimates. For instance, rotation causes the individual beams in a multi-beam to deviate (from the optimal direction) by the same angle at the user. In contrast, if the user undergoes translation, the individual beams on the receiver undergo different angular deviations for each beam. Said differently, the amplitude change for each beam would be different over time as the angular deviation is different for each beam.

Model for angular deviation due to user rotation: Consider a multi-beam pattern with K beams at the user (receiver) as well as at the gNB (transmitter). The beams are initially aligned towards LOS or strong reflectors at the beginning of the user motion. As the user rotates, the beam at the user gets misaligned due to rotation, but since the user does not translate, the beams at the gNB will remain aligned with the user (Figure 10(a)). We, therefore, estimate the angle of rotation and proactively refine the beams at the user.

mmReliable uses the CIR to report per-beam power $P_k(t)$ for each OFDM packet received over time t , where $k = 1, \dots, K$ is the individual beam index in multi-beam pattern. $P_k(t)$ can be modeled as (A detailed model is presented in Appendix B):

$$P_k(t) = G_T(\phi_k) + G_R(\theta_k + \varphi(t)) + P_T - P_h \text{ (in dB)}, \quad (13)$$

where $G_T(\phi_k)$ and $G_R(\theta_k)$ are the received and transmit antenna gains along the Angle of Departure (AoD) ϕ_k and Angle of Arrival (AoA) $\theta_k + \varphi(t)$ respectively. Recall that all the individual beams in the user’s multi-beam pattern deviate by the same angle when the user rotates, and is captured by $\varphi(t)$ ($\varphi(0) = 0$) in the AoA. P_T is the transmit power, and P_h is the loss due to wireless channel. The channel loss P_h can be due to path loss or reflection loss, and can be assumed to be static for a small duration of user rotation. To eliminate the unknown channel loss, we calculate the relative power decay in power, from $t = 0$ to $t = t_0$ as

$$P_k(t_0) - P_k(0) = G_R(\theta_k + \varphi(t_0)) - G_R(\theta_k) \text{ (in dB)}. \quad (14)$$

We see that the relative power decay depends only on the user’s antenna pattern $G_R(\cdot)$. Intuitively, the beam pattern is usually symmetric, and two possible values $\varphi(t_0)$ and $-\varphi(t_0)$ could have caused the observed change in G_R . To deal with the ambiguity of the direction of rotation, mmReliable tries one of the two possibilities using CSI-RS probing in the hope that it improves the SNR. If it doesn’t improve SNR, possibly the other angle is correct, and thus,

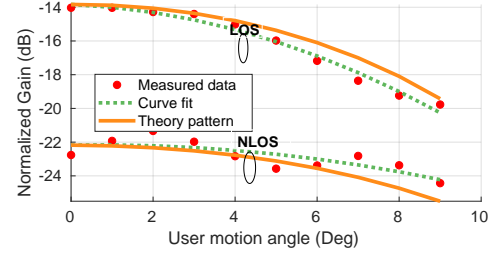


Figure 11: Effect of noise and channel impairments on user tracking for the rotation case. We show that even the NLOS path with low signal strength can be tracked effectively.

mmReliable refines the beam to that angle. The refinement adds an overhead of only one additional probe in addition to $2(K - 1)$ probes required for constructive combining for the K -beam case. mmReliable periodically estimates the value of the per-beam angle, phase, and amplitude and updates the beam pattern at the UE to realign towards the gNB.

Model for angular deviation under user translation: In contrast to the rotation case, translation causes misalignment at both the gNB and the user. Interestingly, we notice that the angular deviation, $\varphi_k(t)$, is the same at both the gNB and the user (See Figure 10(b)). The received power $P_k(t)$ for translation case can be written as

$$P_k(t) = G_T(\phi_k + \varphi_k(t)) + G_R(\theta_k + \varphi_k(t)) + P_T - P_h \text{ (in dB)}. \quad (15)$$

Since the transmit and receive beam patterns are known, the relative power decay can be obtained as:

$$P_k(t_0) - P_k(0) = G_T(\phi_k + \varphi(t_0)) - G_T(\phi_k) + G_R(\theta_k + \varphi(t_0)) - G_R(\theta_k) \text{ (in dB)} \quad (16)$$

Similar to the case in rotation, we have two possible solutions of $\varphi_k(t)$, which can be resolved similarly to the rotation case.

We note from Eq (16) that the receiver needs to know the transmit beam pattern for beam tracking. Fortunately, the beam patterns can be shared with low overhead through the 5G NR control channel. The overhead is low because a multi-beam pattern is generated through a weighted combination of single beam patterns, which are stored in the codebook. The transceiver can share their codebook once, and then they only need to share the codebook index and relative weights of multi-beam pattern in real-time.

Effect of noise and channel impairments: We show that the received signal strength for individual beams in a multi-beam can be tracked accurately. Recall that mmReliable assumes that the wireless channel remains stable for the duration of tracking, and the Received Signal Strength (RSS) follows the shape of the beam pattern.

The tracking of direct path power is not affected by multi-paths due to the sparsity of mmWave channel and the use of highly directional antennas [45, 68]. Also, the power decay due to other factors such as path-loss and noise is not significant for the short duration of tracking. For example, consider a typical V2X scenario with a direct-path link at 20 m. Consider the vehicle is moving with a speed of 20 m/s along a direction perpendicular to the direct path link. For this scenario, we calculate the power decay due to beam

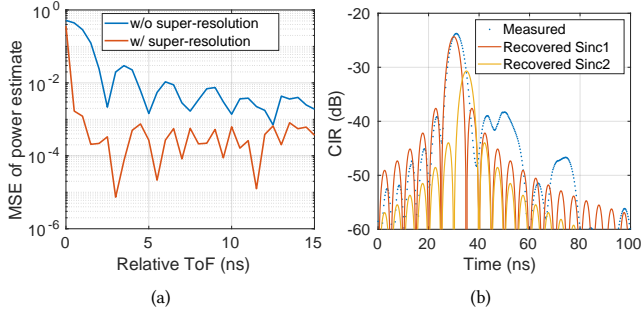


Figure 12: Efficiency of superresolution algorithm: (a) Simulation: Superresolution provides low MSE of per-beam power estimate even when the relative ToF is less than system resolution of 2.5 ns. (b) Hardware measurement: shows two sincs can be recovered from measured combined CIR.

misalignment is 2.1 dB in 100 ms, while the path-loss causes only 0.1 dB decay [22], which is insignificant.

We show in Figure 11 for the rotation case that the measured RSS data indeed follows the theory beam pattern and oscillates around the mean value. Therefore, mmReliable first takes the time average of RSS with a forgetting factor as the user moves and then fits a quadratic polynomial to smoothen the RSS values. We show our curve-fitting on the measured data that, upon proper scaling, approximates the beam pattern well within 1 dB error (Figure 11).

5.3 Superresolution: Improving Per-Beam Tracking

Due to the bandlimited nature of practical systems, we do not have an infinite resolution to tease apart individual beams in a multi-beam at the receiver. Therefore, we present a sinc interpolation approach to recover per-beam amplitude from combined multi-beam channel response and show its importance for user tracking. When receiving a multi-beam transmission, it can be shown that the signal at the receiver consists of a superposition of a delayed and attenuated version of each individual transmit beam. If we consider the delay and attenuation experienced by beam-index k as δ_k and α_k respectively, then the effective multi-beam channel can be expressed as:

$$h_{\text{eff}} = \sum_k \alpha_k \delta(t - \tau_k), \quad (17)$$

Where α_k is a function of the transmitter and receiver beam pattern, while δ_k relates to the Time of Flight (ToF) of each multi-beam channel path. Recall that our goal is to estimate the individual α_k for each beam ($k = 1, \dots, K$).

For a frequency-selective wideband system the received signal is sampled at sampling rate and sinc interpolated due to limited bandwidth as follows:

$$h_{\text{eff}}[n] = \sum_k \alpha_k \text{sinc}(B(nT_s - \tau_k)) \quad (18)$$

where B is the bandwidth of the waveform, T_s is the sampling rate of the receiver, and α_k is total signal attenuation along path k .

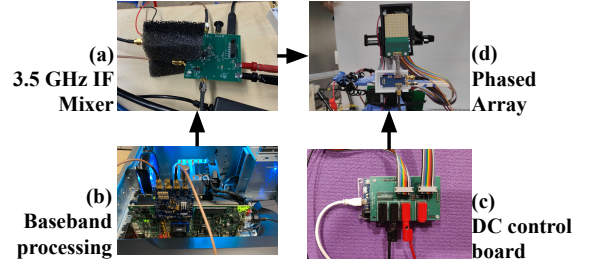


Figure 13: We custom design a testbed at 28 GHz with 64 element phased array and an FPGA board for baseband processing.

We can re-write the above formulation as an optimization problem where our objective is to find α_k such that it fits the channel best. Let say the collected CIR is represented by column vector \mathbf{h} . We solve the following optimization to extract $\alpha = [\alpha_1 \alpha_2 \dots \alpha_K]^T$, which amplitude per beam.

$$\alpha_{\text{est}} = \arg \min_{\alpha} \|\mathbf{h} - \mathbf{S}\alpha\|^2 + \lambda \|\alpha\|^2 \quad (19)$$

where the matrix \mathbf{S} consists of all the ToF. We are essentially solving a super-resolution problem by fitting a sinc model over the entire CIR response. The optimization is a convex formulation, with L2 norm regularization. We use standard techniques [31] to solve this problem in $100\mu\text{s}$. Here, we make a key observation that, after training, the absolute ToF may have changed, but the relative ToF changes slowly. Our key idea is that we shift the \mathbf{h} first so that the strongest path is shifted to zero delays and since we know relative to the first path, the delay of the second and third path. We can populate the \mathbf{S} matrix with only a few columns, thereby achieving accurate and reliable solutions to α_k . We account for the small variations in relative-ToF by trying a few values around the initial value that best fits our model. In summary, we have built an accurate super-resolution algorithm by leveraging the initial relative-ToF information between the multi-beams.

Efficiency of super-resolution algorithm: In Figure 12(a), we show that our super-resolution algorithm can indeed achieve high resolution in estimating per-beam amplitude even when the relative ToF is lower than what corresponds to the resolution (2.5 ns for 400 MHz bandwidth). We also measure the channel impulse response through our testbed (6m link with a reflector placed at 30°) in Figure 12(b) and show that our super-resolution can efficiently extract the two sinc which are superimposed in the received CIR.

6 IMPLEMENTATION

We build a custom mmWave testbed at 28 GHz to evaluate the performance of mmReliable as shown in Figure 13. The testbed [37] consists of three main components: (i) Baseband processing module: Gsps digital and analog front-end unit (Analog Devices FMC-DAQ2 [3]) connected to a bespoke Baseband processing unit FPGA (Xilinx KCU105) [4], which is connected to the host PC. (ii) IF module: connects with baseband processing module and consists of the Mixer (Qorvo RFFC5071A [9]), a High Pass Filter (Mini-Circuits ZFHP-3800ff-S+ [6]) and a 15 dB LNA (Mini-Circuits ZX60-P103LN+ [7]). (iii) Tx/Rx module: connected with the IF module and consists of up-down converters and Tx/Rx transceivers, which are connected to Phased Array Antennas [42], and the DC beam control



Figure 14: Outdoor and Indoor test scenarios. The far right figure shows our phased array mounted on a gantry system which provides precise translation and rotation motion ground truth information.

board. We also used a 28 GHz horn antenna (Pasternack PE9851/2F-10 [8]) for antenna calibration and measuring beam patterns. We generate OFDM waveforms with 400 MHz effective bandwidth for our evaluation. A host PC handles pre/post data processing and waveform generation. A MATLAB controlled Arduino SPI platform is used to interface with the phased array and enables fast switching of beam patterns.

7 EVALUATION

Figure 14 shows our hardware set-up and evaluation scenarios. We evaluate the performance of mmReliable in two indoor and outdoor settings: a large $7m \times 10m$ conference room occupied with wooden furniture, whiteboard, and reflective glass walls, and another relatively less occupied $6m \times 6m$ lab space and outdoors. We set up the communication link at $7m$ and $4m$ at the two rooms, respectively, and $30m$ outdoors. The Tx module of the testbed is used to emulate a fixed gNB while the Rx module is movable and emulates a mobile user placed on a cart. The phased array antenna of the Tx is kept vertical, facing the user, and parallel to the line of user translation. We used a Cinetics Axis-360 [5] gantry system to measure the precise ground truth of user motion. The precision gantry setup allows 70 cm linear motion and 360-degree rotation about its axis accurate to 1 cm and 0.1° , respectively. The Rx phased array mounted on the gantry (see Figure 14 rightmost image) emulate a mobile user with $24^\circ/\text{s}$ rotation (typical speed for VR headset motion [51]) and 1.5 m/s translation speed in indoor scenarios. For outdoor experiments, we manually move the cart to predefined grid locations for accurate ground truth information.

We perform multiple experiments of a 1-sec duration of user mobility. At the beginning of each experiment, we perform beam training to establish directional communication and estimate initial parameters such as AoA, AoD, ToF, and reflector attenuation. Our testbed reports the Signal to Noise Ratio (SNR) of the wireless link and data rates using 400 MHz bandwidth similar to other testbeds [68, 69, 85].

Figure 14 shows our hardware set-up and evaluation scenarios. We evaluate the performance of mmReliable in two indoor and outdoor settings: a large $7m \times 10m$ conference room occupied with wooden furniture, whiteboard, and reflective glass walls, and another relatively less occupied $6m \times 6m$ lab space and outdoors. We set up the communication link at $7m$ and $4m$ at the two rooms, respectively, and $30m$ outdoors. The Tx module of the testbed is used to emulate a fixed gNB while the Rx module is movable and emulates a mobile user placed on a cart. The phased array antenna of the Tx is kept vertical, facing the user, and parallel to the line of user translation. We used a Cinetics Axis-360 [5] gantry system to measure the precise ground truth of user motion. The precision

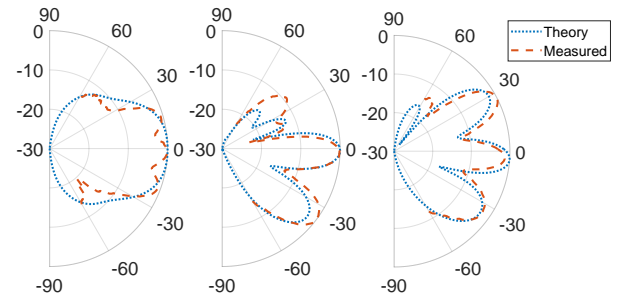


Figure 15: Beam patterns measured through our phased arrays in an anechoic chamber (a) Wide single-beam pattern, (b) 2-beam pattern, and (c) 3-beam pattern.

gantry setup allows 70 cm linear motion and 360-degree rotation about its axis accurate to 1 cm and 0.1° , respectively. The Rx phased array mounted on the gantry (see Figure 14 rightmost image) emulate a mobile user with $24^\circ/\text{s}$ rotation (typical speed for VR headset motion [51]) and 1.5 m/s translation speed in indoor scenarios. For outdoor experiments, we manually move the cart to predefined grid locations for accurate ground truth information.

We perform multiple experiments of a 1-sec duration of user mobility. At the beginning of each experiment, we perform beam training to establish directional communication and estimate initial parameters such as AoA, AoD, ToF, and reflector attenuation. Our testbed reports the Signal to Noise Ratio (SNR) of the wireless link and data rates using 400 MHz bandwidth similar to other testbeds [68, 69, 85].

7.1 Micro Benchmarks

We will first show that effective multi-beams can be generated from our mmWave testbed and then characterize our system, providing benchmarks for both constructive combining and proactive user tracking.

7.1.1 Generating multi-beam patterns. Recall that we generate multi-beam patterns by taking a weighted average of the corresponding single beams with weights proportional to attenuation of the path along the beam direction. We then normalize the gain at each antenna to a constant total radiated power (TRP) in all cases of single or multi-beam. Table 2 shows the EIRP achieved by different single or multi-beam (with attenuation, $\delta = -3\text{ dB}$) for the same TRP of 30 dBm . For 2-beam cases, we observe that the power is distributed along two beams, causing an EIRP loss of 1.7 dB compared to a single beam. Despite low EIRP, the multi-beam delivers higher throughput when combined with our novel constructive combining as detailed in later evaluation. Finally, Figure 15 shows that our

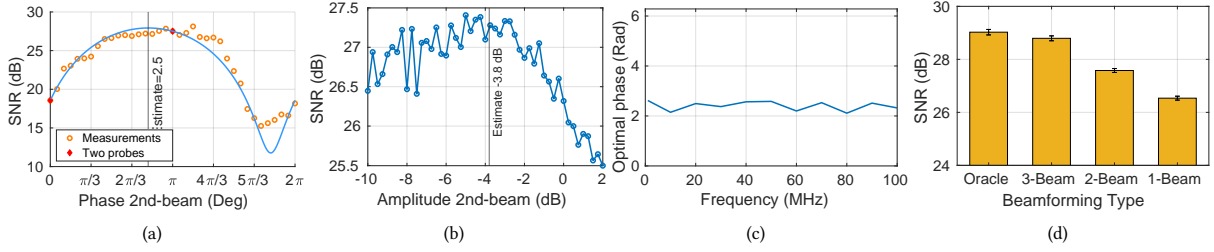


Figure 16: (a) SNR measurements with different phases of the 2nd beam in our 2-beam pattern, (b) SNR measurements with various amplitudes of the 2nd beam through brute-force probing. We also show that our constructive combining requires only two probes and provides accurate phase and amplitude estimates without brute-force scanning. (c) The optimal phase is stable over a frequency range of 100 MHz. (d) SNR gain of multi-beam against single beam and oracle (knows the best channel-dependent beam) for a static unblocked link.

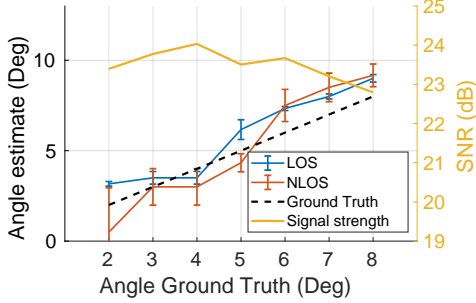


Figure 17: Tracking angle accuracy: shows mmReliable can estimate the angle within 1° error.

phased arrays with 27 dB of gain control and 6-bit phase control indeed achieve accurate multi-beam patterns compared against simulation.

| Beam Angle | 0° | $0^\circ, 30^\circ$ | $0^\circ, 45^\circ$ | $0^\circ, -30^\circ, 45^\circ$ |
|------------|-----------|---------------------|---------------------|--------------------------------|
| TRP (dBm) | 30 | 30 | 30 | 30 |
| EIRP (dBm) | 27.7 | 26 | 26 | 24.7 |

Table 2: Total Radiated Power and per-beam EIRP for various single and multi-beams.

7.1.2 Constructive combining accuracy. We first show the need for constructive combining in a multi-beam system and then evaluate the performance of mmReliable’s novel algorithm for estimating the phase ζ and amplitude δ needed for constructive combining. We establish a multi-beam link with two beams towards a static UE with our indoor 7m link set up. We direct the first beam along the LOS path with phase unity and amplitude of 0 dB. We then perform an exhaustive scan of the second beam’s phase in the range $[0, 2\pi]$ and observe the SNR variations. Figure 16(a) shows that the SNR variations can be as large as 13 dB, which motivates the need for constructive combining. It also indicates that mmReliable’s two-probe method accurately estimates the phase of 2.5 radians, which maximizes the SNR. Similarly, we perform an exhaustive scan of the second beam’s amplitude in the range of $[-10, 2]$ dB and show the SNR variations in Figure 16(b). It indicates that the SNR is highest for a range of amplitude around -5 dB to -3 dB. Therefore the estimate of -3.8 dB using the two-probe method is reasonably accurate. Finally, we show the per-beam phase’s stability over the 100 MHz frequency range in Figure 16(c). We observe that phase

variation is less than 1 rad, which doesn’t impact the SNR gain of our multi-beam system.

7.1.3 SNR gain due to constructive combining. We now verify that the constructive combining of multi-beams leads to higher SNR than a single beam system even for a static unblocked link. We reuse our previous set-up and establish a multi-beam with either 2 or 3 beams aligned with the LOS path at 0° and two reflectors (a metal sheet and a white board) at -30° and 20° respectively. We also create an oracle beam pattern, the best channel-dependent pattern which knows the channel per-antenna element in the phased array. To measure the channel per-antenna, we turn on two antennas and send four probes with different phase-shifts to measure the relative complex channel across the two antennas and repeat the process for all the antennas. The receiver beam pattern is kept omnidirectional in each experiment. We emphasize that all the beam patterns are quantized to satisfy the phased array’s resolution and scaled to meet the TRP constraint. We observe in Figure 16(d) that the single beam pattern is not the optimal choice for such a channel. The oracle channel-dependent beams can provide 2.5 dB better SNR compared to the single-beam. The 3-beam link also provides 2.27 dB higher SNR than the single-beam, providing gains close to the oracle. Even the two-beam link outperforms a single beam by 1.04 dB. *This analysis indicates that 3-beams are enough to provide close to 92% gains of the optimal beam with significantly less overhead than the oracle solution.*

7.1.4 Rotation angle estimation accuracy. We first find out whether our amplitude-based tracking can estimate accurate angular motion. We also want to know how often our system performs beam refinement to maximize the SNR. To evaluate these results, we set up a link at 7m to perform multiple experiments with a uniform rotation of the Rx array. The frequency of rotation is varied over a range of 2 degrees to 8 degrees, and the average angle estimate is reported in Figure 17. We observe that the mean angle estimate is accurate to 1° . In the same figure, we also plot the SNR of each tracking experiment. We observe the SNR is maximum when the tracking frequency is every 4 degrees (corresponding to 1.5 dB of power decay for our 64 elements phased array). For the rest of the evaluation, we perform beam refinement when the system detects a power decay of 1.5 dB per-beam in the multi-beam setup.

7.1.5 Tracking accuracy time series. We show how our multi-beam tracking and constructive combining improves the SNR of

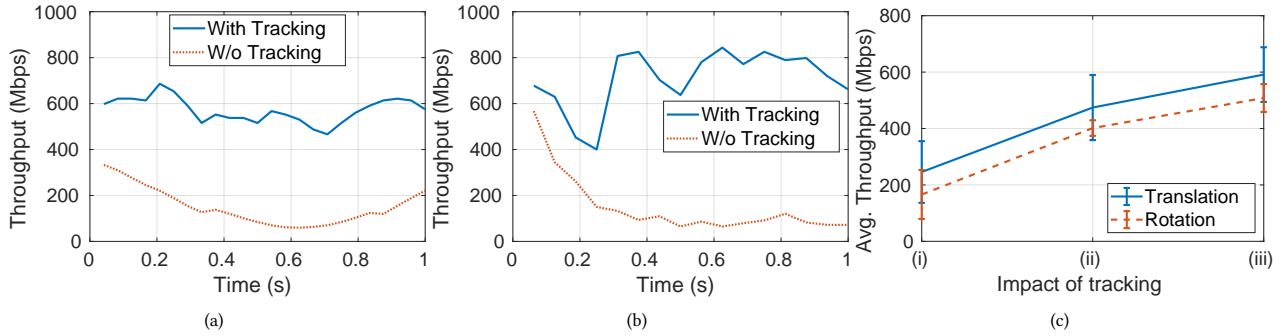


Figure 18: Effectiveness of tracking: (a) Rotation time series, (b) Translation time series. (c) Average Throughput gain (i) No Tracking, (ii) With Tracking (iii) Tracking plus constructive combining.

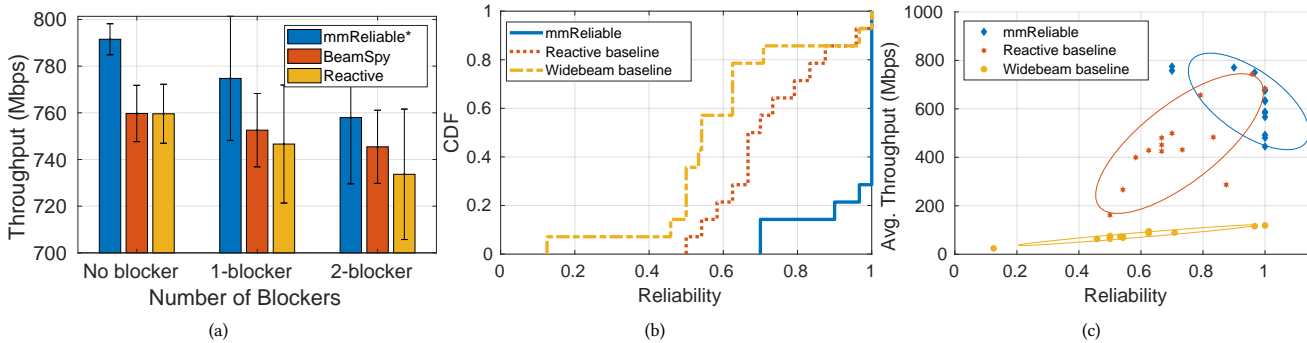


Figure 19: End-to-end performance gain of mmReliable compared to baselines: (a) Static link with blockages (*evaluates mmReliable without proactive user tracking) (b) Reliability for mobile link (b) Overall Throughput-Reliability Trade-off.

the wireless link and prevents it from falling to outage despite user mobility.

Tracking Rotation: We rotate the user on its axis for up to 24 degrees equivalent to 1-sec rotation motion. mmReliable rotation tracking improves the average throughput by around 400 Mbps (4x on average) as compared to multi-beam with no tracking, as shown in Figure 18(a). Thus, proving that the tracking algorithm works for rotation scenarios.

Tracking Translation: The user is translated using the gantry system without any obstructions. We show that mmReliable tracking improves the average throughput by 350 Mbps over multi-beam without tracking, as shown in Figure 18(b). Thus, proving that the tracking algorithm works for translation scenarios as well.

7.1.6 Advantage of tracking and constructive combining algorithm. The effect of tracking and constructive combining is individually investigated in Figure 18(c). We observe that tracking alone (without constructive combining) improves the throughput by 2x for rotation and translation compared to the case without any tracking. Furthermore, the constructive combining on top of the tracking improves the throughput gain by an additional 1.25x compared to results with only tracking. We see a similar improvement in throughput in both translation and rotation cases.

7.2 End-to-end Results

7.2.1 Multi-beam performance for static link: We first show that a multi-beam link can outperform a single-beam link during regular operation (static user with occasional blockages) with appropriate

power-control and constructive combining. We establish an indoor setup with a 5m link and a metallic reflector present at 30° from the LOS. Figure 19(a) shows that mmReliable delivers 31 Mbps higher throughput using phase-coherent multi-beam compared to a single directional beam with the same total radiated power. Even in a completely static link with no blockages, mmReliable optimizes the multi-beam to take advantage of the reflected path and increase throughput as described in Section 3. We then introduce blockage that appears at a random time, and each blocker blocks the link for roughly 10% of the experiment duration. We compare the throughput performance against two baselines, BeamSpy [69], which finds the best un-blocked link without scanning overhead and the best reactive baseline [34], which react to blockages by performing a fast scan. We show that mmReliable consistently outperforms the two baselines for all blockage scenarios. mmReliable’s throughput drops only by 4% when two blockers block the link because of the proactive utilization of the reflectors. Beamspy can also handle blockages efficiently, but it consistently provides low throughput compared to mmReliable. The reactive baseline suffers from high probing overhead to maintain a high throughput link. Thus, mmReliable outperforms traditional systems for a static link with occasional blockages.

7.2.2 Improvement in Reliability for mobile links. We perform user translation and rotation experiments to emulate practical occurrences in environments. As the user moves, a human blocker is introduced midway between Tx and Rx, blocking the link for a duration chosen uniformly between 100 ms to 500 ms [55], over

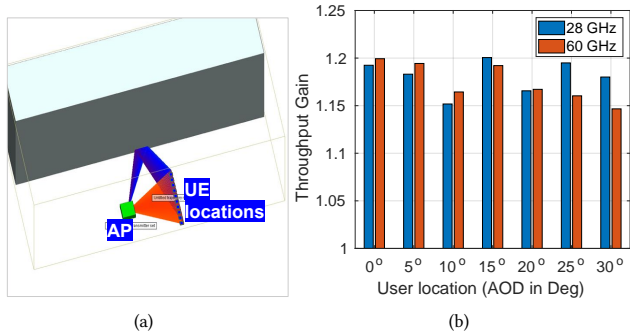


Figure 20: (a) Wireless Insite simulation scenario, (b) Throughput Gain comparing 28 GHz and 60 GHz system for static UE with 10% blockages.

1-sec experiments. We perform 100 such experiments and combine the results to form one point, and various user mobility and blockage patterns across two indoor environments are reported on the throughput and reliability curve. Figure 19(b) shows that mmReliable achieves close to 100% reliability. The reactive baseline suffers from lower reliability of mean 0.65, while the widebeam baseline is at 0.45. Thus, mmReliable achieves its goal of high-reliability.

7.2.3 Throughput-Reliability Trade-off. We finally introduce a new metric to evaluate a mmWave system, which plots the data collected in the last sub-section with a two-dimensional plot for both reliability and throughput. We also compare the throughput of mmReliable with other baselines in Figure 19(c). We show that mmReliable does not suffer from throughput loss, while the other benchmarks suffer from throughput degradation due to the user’s mobility. The results indicate that mmReliable delivers an average throughput of 200 Mbps more than that achieved by the reactive baseline (average of 400 Mbps), 50% more throughput than reactive baseline. More importantly, mmReliable offers a consistent throughput with low variations compared to the baseline, essential to many mission-critical applications. Thus, mmReliable can achieve a high-reliability link similar to sub-6 GHz communication while taking advantage of mmWave high data rates. Furthermore, the average reliability is 1 for mmReliable, compared to the comparative benchmark whose reliability is 0.65. In summary, we introduce a new metric to evaluate a mmWave system, which shows both reliability and throughput. *The evaluation reveals that mmReliable is advantageous over throughput-based design on both throughput and reliability.*

7.2.4 Study of 60 GHz network: We now show that mmReliable presents a general framework to improve mmWave throughput and reliability that can also be applied to a 60 GHz network. To compare the two systems, we perform a simulation study using Wireless Insite [60], as shown in Figure 20. We establish a directional link at 10m with a reflecting surface (made up of concrete material) at 60° (Figure 20(a)). We set other simulation parameters according to a recent large-scale study of a 60 GHz system [75]. The results in Figure 20(b) show that mmReliable outperforms single-beam based baseline [69] by 1.18× gain in throughput for static UE with 10% blockages. Both 28 GHz and 60 GHz system performs similarly, and the result is consistent across multiple UE locations. Nonetheless,

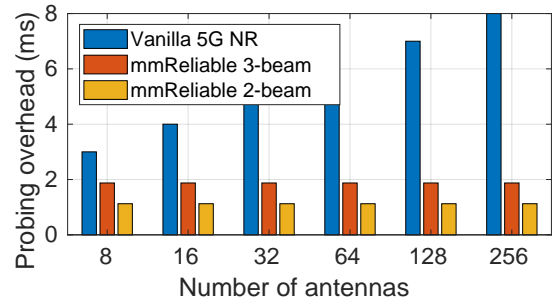


Figure 21: Probing overhead of mmReliable is low compared to vanilla 5G NR system.

28 GHz throughput is 4.7× higher than 60 GHz (not shown) for the same bandwidth since 60 GHz links suffer from higher path loss and attenuation due to environmental absorption.

7.2.5 Beam probing overhead. mmReliable reduces the beam probing overhead by maintaining a multi-beam link through tracking and beam refinements. The proposed beam refinement procedure requires two probes for constructive combining (2-beam case) and one probe for detecting the direction of motion, thus requiring a total of 3 CSI-RS probes. For the 3-beam case, it only increases to 5 probes. On the other hand, an entire beam scan using SSB in traditional 5G NR requires a large number of SSB probes proportional to the number of spatial directions. One CSI-RS occupies one slot, which is 0.125 ms at 120 kHz sub-carrier spacing, and one SSB takes four slots (0.5 ms). Let’s consider the best scanning method, which requires number of probes proportional to only a logarithmic number of antennas. We show in Figure 21 the overall probing latency assuming an average of three refinement phases can replace a single beam acquisition. We see that traditional 5G NR suffers from higher probing overhead compared to mmReliable. The 5G NR probing overhead for 8 antennas is 3 ms, which increases to 8 ms for 256 antennas (because of the high-directionality of beam patterns). In contrast, the overhead of mmReliable remains as low as 1.1 ms for 2-beam and 1.9 ms for 3-beam cases independent of the number of antennas. *Thus, mmReliable is an efficient solution for beam management, which improves mmWave link reliability and throughput while maintaining low system overhead.*

8 RELATED WORK

mmReliable is closely related to extensive work in mmWave communication literature, therefore we have grouped the past work into following categories.

Channel-dependent beamforming: Multi-beam patterns belong to the family of channel-dependent beamforming [48, 65] where the beamforming weights are obtained to maximise the SNR for a given channel condition. For instance, [65] showed through channel sounding measurements that combining multiple signals across four directions could achieve 28 dB improvement in pathloss at 28 GHz. Traditionally these optimizations are proposed for a MIMO system which uses channel measurements at each antenna [24, 25, 35] for digital beamforming. In contrast, mmReliable focus on analog

beamforming where the signal from each antenna elements are connected through a single RF chain. ACO [48] proposed a procedure to estimate the per-antenna CSI on an analog array by designing a specific beam scan procedure. However, it suffers from high overhead proportional to number of antennas and so the procedure cannot be repeated very often when the channel changes. In contrast, we propose multi-beams which approximates the optimal beam pattern and are easy to maintain with low overhead.

Blockage and mobility: BeamSpy [69] and Beam-forecast [83] provide a model-driven approach to handle blockage and mobility, respectively. However, they lack a unified framework to integrate both vulnerabilities and also suffer from high run-time optimization and table-lookup complexity. To recover from a complete outage, UBig [67] performs efficient handovers and mmChoir [78] proposes joint transmission from multiple base stations. These approaches may improve system reliability but add additional signaling overhead. Moreover, the fundamental difference is they use a single beam and are reactive. In contrast, mmReliable proposes a mmWave system which utilizes multipath aware multi-beam patterns that are realigned proactively; therefore facilitating reliable and stable links without requiring additional signaling.

AoA estimation and tracking: Location estimation using CSI from single or multiple gNBs can be used for both sensing and beam management [26, 33, 49, 50, 57]. mmReliable’s AoA estimation is built on the insights from these works but differ in the sense that mmReliable doesn’t need to estimate the user location but only the direction which requires only one gNB. Moreover, mmReliable extends the past work to estimate direction of not only the direct path but it also simultaneously tracks all the multi-paths without requiring beam scan, but by leveraging unique multi-beam channel estimates. Moreover, mmReliable avoids frequent AoA estimation from tedious beam scan and follows the approach of beam tracking with negligible overhead. [43] developed a mechanism to detect direction of user movement and adjust beam direction in small increments. Though they use 2-lobe pattern to detect mobility, they switch back to single-beam pattern for communication.

Beam Training: Beam training based on exhaustive search [20, 38, 84], hierarchical search [21, 68, 84] incurs high delay proportional to the number of antennas which is significantly high for large phased arrays. For faster beam acquisition, [15, 18, 19, 34, 72] recently proposed to simultaneously use multiple beams to reduce the search space from linear to logarithmic in terms of number of discrete spacial directions. However, they focused on initial beam training of the system. In contrast, mmReliable focuses on link maintenance and reliability and therefore is complementary to initial beam training approaches. A similar system [18] proposes phase-coherent multi-beams for communication that is evaluated with simulations and lacks an end-to-end system design with beam tracking, constructive combining and super-resolution required for a practical system.

High training overhead may be reduced by taking assistance from device positioning systems [74, 76, 80] or light sensors [32], out-of-band WiFi [46, 66], and multi-user coordination techniques [52, 64]. However, in contrast to mmReliable, they suffer from relatively lower accuracy with added complexity while being dependent on external devices. mmReliable high accuracy is achieved based

on the super-resolution algorithm combined with motion tracking algorithm.

Reflecting surfaces: Prior work on active mmWave relay [14, 70] requires additional active devices (antenna array) with beamforming capabilities to relay the signal towards the user. These devices add up to the cost and power requirements. On the other hand, mmReliable relies entirely on natural reflectors present in the environment. Furthermore, mmReliable can leverage such active mmWave relays to create multi-beam and augment them with constructive combining, proactive tracking and adaptation algorithms. The authors of [27, 41, 79, 85] leverage reflective surfaces to improve indoor mmWave connectivity and coverage based on simulation models. [86] exploits outdoor reflections for a robust NLOS link. E-Mi [77] and mmRanger [82] provide models to estimate the reflector parameters in a realistic environment. However, they require tedious environment mapping by moving the client manually or by placing it on an autonomous bot. Their model is suitable for one-time sensing for initial network deployment, which complements with our goal of improving the link reliability in real-time.

9 LIMITATIONS AND FUTURE WORK

Multi-beams with constructive combining and proactive tracking enables reliable, high throughput mmWave links. Since multi-beams are a new class of beamforming itself, designing a robust networking system while multiplexing multiple users is an open challenge. We mention some limitations of our work and lay the ground for future work.

Robust tracking: We provide a model for tracking the angle of rotation and translation based on per-path amplitude estimates. For a small duration of tracking, the motion can be piece-wise divided into translation or rotation of the user, but a complex motion may have both at the same time. Our initial idea is to exploit other channel dimensions such as time-of-flight and Doppler estimation for robust tracking, which we leave for our future work.

Multi-user and MIMO setup. MIMO helps in enhancing the diversity of single-user link, or it can enhance the multiplexing of multiple users. Prior work [28, 40] has proposed interference-aware spatial multiplexing of beams in different directions for multiple users. mmReliable can be combined with the above work to provide reliability to multiple clients at the same time and enable proactive tracking of multiple clients. In particular, some of the spatial beams can be used for enhancing the reliability of single-user while other beams can be used to improve the performance of multi-user.

10 CONCLUSION

In this work, we present first throughput and reliability oriented mmWave systems, which has been evaluated with a high-speed base-band with 400 MHz and 8x8 antenna arrays in realistic environmental setup and showed the ability to achieve reliability close to 1 and throughput gain of 1.5x. This work provides insights on how using multi-beam can enable user tracking without any side-channel information. Furthermore, the proactive approach to tracking has the potential to truly enable reliable mmWave. We believe this work paves the way for a new direction in mmWave where environmental reflections and careful channel estimation can improve beam management.

REFERENCES

- [1] IEEE 802.11ad: Enhancements for Very High Throughput in the 60 GHz Band. *IEEE*, 2009.
- [2] Verizon to test 5G at 28 GHz in Texas with Samsung. <https://www.fiercewireless.com/tech/verizon-to-test-5g-at-28-ghz-texas-samsung>, Feb 2016.
- [3] Analog Devices, AD-FMCDQA2-EBZ. <https://wiki.analog.com/resources/eval/user-guides/ad-fmcdqa2-ebz>, Sept. 2019.
- [4] Analog Devices, KCU 105. <https://www.xilinx.com/products/boards-and-kits/kcu105.html>, Sep 2019.
- [5] Cinetics axis-360 motion control system. <https://cinetics.com/axis360-pro/>, Sep 2019.
- [6] Mini-Circuits ZFHP-3800FF-S+. <https://www.minicircuits.com/pdfs/ZFHP-3800FF-S+.pdf>, Sept. 2019.
- [7] Mini-Circuits ZX60-P103LN+. <https://www.minicircuits.com/pdfs/ZX60-P103LN+.pdf>, Sept. 2019.
- [8] Pasternack PE9851/2F-10. <https://www.everythingrf.com/products/waveguide-horn-antennas/pasternack-enterprises-inc/617-20-pe9851-2f-10>, Sept. 2019.
- [9] Qorvo, RFFC5071A: 85 - 4200 MHz Wideband Synthesizer / VCO with Integrated 6 GHz RF Mixer. <https://www.qorvo.com/products/p/RFFC5071A>, Sept. 2019.
- [10] Talon AD7200 Multi-Band Wi-Fi Router. <https://www.tp-link.com/us/home-networking/wifi-router/ad7200/>, Sep 2019.
- [11] 5G NR (New Radio) Release 16. 3GPP. <https://www.3gpp.org/release-16>, Jul 2020.
- [12] IBM device paves the way for 5G to reach full potential. <https://www.ibm.com/blogs/research/2020/06/ibm-device-5g-full-potential/>, Jun 2020.
- [13] 3GPP. 5G NR (New Radio) Release 15. 3GPP. <https://www.3gpp.org/release-15>, Oct 2019.
- [14] O. Abari, D. Bharadia, A. Duffield, and D. Katabi. Enabling high-quality untethered virtual reality. In *14th {USENIX} Symposium on Networked Systems Design and Implementation ({NSDI} 17)*, pages 531–544, 2017.
- [15] O. Abari, H. Hassanieh, M. Rodriguez, and D. Katabi. Millimeter wave communications: From point-to-point links to agile network connections. In *HotNets*, pages 169–175, 2016.
- [16] A. Alkhateeb, O. El Ayach, G. Leus, and R. W. Heath. Channel estimation and hybrid precoding for millimeter wave cellular systems. *IEEE Journal of Selected Topics in Signal Processing*, 8(5):831–846, 2014.
- [17] C. R. Anderson and T. S. Rappaport. In-building wideband partition loss measurements at 2.5 and 60 GHz. *IEEE transactions on wireless communications*, 3(3):922–928, 2004.
- [18] I. Aykin, B. Akgun, and M. Krunz. Multi-beam transmissions for blockage resilience and reliability in millimeter-wave systems. *IEEE Journal on Selected Areas in Communications*, 37(12):2772–2785, 2019.
- [19] I. Aykin, B. Akgun, and M. Krunz. Smartlink: Exploiting channel clustering effects for reliable millimeter wave communications. In *IEEE INFOCOM 2019-IEEE Conference on Computer Communications*, pages 1117–1125. IEEE, 2019.
- [20] C. N. Barati, S. A. Hosseini, M. Mezzavilla, P. Amiri-Eliasi, S. Rangan, T. Korakis, S. S. Panwar, and M. Zorzi. Directional initial access for millimeter wave cellular systems. In *Signals, Systems and Computers, 2015 49th Asilomar Conference on*, pages 307–311. IEEE, 2015.
- [21] C. N. Barati, S. A. Hosseini, M. Mezzavilla, T. Korakis, S. S. Panwar, S. Rangan, and M. Zorzi. Initial access in millimeter wave cellular systems. *IEEE Transactions on Wireless Communications*, 15(12):7926–7940, 2016.
- [22] T. Chen, M. Kohli, T. Dai, A. D. Estigarribia, D. Chizhik, J. Du, R. Feick, R. A. Valenzuela, and G. Zussman. 28 GHz channel measurements in the COSMOS testbed deployment area. In *Proceedings of the 3rd ACM Workshop on Millimeter-wave Networks and Sensing Systems*, pages 39–44, 2019.
- [23] T. Driscoll, S. Farhoud, S. Nowling, et al. Enabling mobile augmented and virtual reality with 5G networks. Technical report, Tech. Rep., Jan, 2017.
- [24] O. El Ayach, R. W. Heath, S. Abu-Surra, S. Rajagopal, and Z. Pi. Low complexity precoding for large millimeter wave MIMO systems. In *2012 IEEE international conference on communications (ICC)*, pages 3724–3729. IEEE, 2012.
- [25] O. El Ayach, S. Rajagopal, S. Abu-Surra, Z. Pi, and R. W. Heath. Spatially sparse precoding in millimeter wave MIMO systems. *IEEE transactions on wireless communications*, 13(3):1499–1513, 2014.
- [26] D. Garcia, J. O. Lacruz, P. J. Mateo, and J. Widmer. Polar: Passive object localization with ieee 802.11 ad using phased antenna arrays. In *IEEE INFOCOM 2020-IEEE Conference on Computer Communications*, pages 1838–1847. IEEE, 2020.
- [27] Z. Genc, U. H. Rizvi, E. Onur, and I. Niemegeers. Robust 60 GHz indoor connectivity: Is it possible with reflections? In *2010 IEEE 71st vehicular technology conference*, pages 1–5. IEEE, 2010.
- [28] Y. Ghasempour. Multi-Stream Beam-Training for mmWave MIMO Networks. In *Proceedings of the 24th Annual International Conference on Mobile Computing and Networking*. ACM, 2018.
- [29] M. Giordani, M. Mezzavilla, C. N. Barati, S. Rangan, and M. Zorzi. Comparative analysis of initial access techniques in 5G mmwave cellular networks. In *Information Science and Systems (CISS), 2016 Annual Conference on*, pages 268–273. IEEE, 2016.
- [30] M. Giordani, M. Polese, A. Roy, D. Castor, and M. Zorzi. A tutorial on beam management for 3GPP NR at mmWave frequencies. *IEEE Communications Surveys & Tutorials*, 21(1):173–196, 2018.
- [31] M. Grant and S. Boyd. CVX: Matlab software for disciplined convex programming, version 2.1. <http://cvxr.com/cvx>, Mar. 2014.
- [32] M. K. Haider, Y. Ghasempour, D. Koutsonikolas, and E. W. Knightly. Lister: Mmwave beam acquisition and steering by tracking indicator leds on wireless aps. In *Proceedings of the 24th Annual International Conference on Mobile Computing and Networking*, pages 273–288. ACM, 2018.
- [33] M. K. Haider and E. W. Knightly. Mobility resilience and overhead constrained adaptation in directional 60 ghz wlans: protocol design and system implementation. In *Proceedings of the 17th ACM International Symposium on Mobile Ad Hoc Networking and Computing*, pages 61–70, 2016.
- [34] H. Hassanieh, O. Abari, M. Rodriguez, M. Abdelghany, D. Katabi, and P. Indyk. Fast millimeter wave beam alignment. In *Proceedings of the 2018 Conference of the ACM Special Interest Group on Data Communication*, pages 432–445. ACM, 2018.
- [35] R. W. Heath, N. Gonzalez-Prelcic, S. Rangan, W. Roh, and A. M. Sayeed. An overview of signal processing techniques for millimeter wave MIMO systems. *IEEE journal of selected topics in signal processing*, 10(3):436–453, 2016.
- [36] IDT. F5280: Transmit/Receive Half Duplex IC 25GHz to 31GHz. <https://www.idt.com/products/rf-products/phased-array-beamformers/f5280-transmitreceive-half-duplex-ic-25ghz-31ghz>, Sept. 2019.
- [37] I. K. Jain, R. Subbaraman, T. H. Sadarahalli, X. Shao, H.-W. Lin, and D. Bharadia. mmobile: Building a mmwave testbed to evaluate and address mobility effects. In *Proceedings of the 4th ACM Workshop on Millimeter-Wave Networks and Sensing Systems*, pages 1–6, 2020.
- [38] C. Jeong, J. Park, and H. Yu. Random access in millimeter-wave beamforming cellular networks: issues and approaches. *IEEE Communications Magazine*, 53(1):180–185, 2015.
- [39] H. Ji, S. Park, J. Yeo, Y. Kim, J. Lee, and B. Shim. Ultra-reliable and low-latency communications in 5G downlink: Physical layer aspects. *IEEE Wireless Communications*, 25(3):124–130, 2018.
- [40] S. Jog, J. Wang, J. Guan, T. Moon, H. Hassanieh, and R. R. Choudhury. Many-to-many beam alignment in millimeter wave networks. In *16th {USENIX} Symposium on Networked Systems Design and Implementation ({NSDI} 19)*, pages 783–800, 2019.
- [41] W. Khawaja, O. Ozdemir, Y. Yapici, I. Guvenc, and Y. Kakishima. Coverage enhancement for mm wave communications using passive reflectors. In *2018 11th Global Symposium on Millimeter Waves (GSMM)*, pages 1–6. IEEE, 2018.
- [42] K. Kibaroglu, M. Sayginer, T. Phelps, and G. M. Rebeiz. A 64-element 28-GHz phased-array transceiver with 52-dBm EIRP and 8–12-Gb/s 5G link at 300 meters without any calibration. *IEEE Transactions on Microwave Theory and Techniques*, 66(12):5796–5811, 2018.
- [43] A. Loch, H. Assasa, J. Palacios, J. Widmer, H. Suys, and B. Debaille. Zero overhead device tracking in 60 GHz wireless networks using multi-lobe beam patterns. In *Proceedings of the 13th International Conference on emerging Networking Experiments and Technologies*, pages 224–237, 2017.
- [44] G. R. MacCartney, T. S. Rappaport, and S. Rangan. Rapid fading due to human blockage in pedestrian crowds at 5G millimeter-wave frequencies. In *GLOBECOM 2017-2017 IEEE Global Communications Conference*, pages 1–7. IEEE, 2017.
- [45] A. Narayanan, J. Carpenter, E. Ramadan, Q. Liu, Y. Liu, F. Qian, and Z.-L. Zhang. A first measurement study of commercial mmwave 5G performance on smartphones. *arXiv preprint arXiv:1909.07532*, 2019.
- [46] T. Nitsche, A. B. Flores, E. W. Knightly, and J. Widmer. Steering with eyes closed: mm-wave beam steering without in-band measurement. In *2015 IEEE Conference on Computer Communications (INFOCOM)*, pages 2416–2424. IEEE, 2015.
- [47] S. J. Orfanidis. Electromagnetic waves and antennas. 2002.
- [48] J. Palacios. Adaptive Codebook Optimization for Beam Training on Off-the-Shelf IEEE 802.11ad Devices. In *Proceedings of the 24rd Annual International Conference on Mobile Computing and Networking*. ACM, 2018.
- [49] J. Palacios, P. Casari, H. Assasa, and J. Widmer. Leap: Location estimation and predictive handover with consumer-grade mmwave devices. In *IEEE INFOCOM 2019-IEEE Conference on Computer Communications*, pages 2377–2385. IEEE, 2019.
- [50] I. Pefkianakis and K.-H. Kim. Accurate 3d localization for 60 GHz networks. In *Proceedings of the 16th ACM Conference on Embedded Networked Sensor Systems*, pages 120–131, 2018.
- [51] F. Qian, B. Han, Q. Xiao, and V. Gopalakrishnan. Flare: Practical viewport-adaptive 360-degree video streaming for mobile devices. In *Proceedings of the 24th Annual International Conference on Mobile Computing and Networking*, pages 99–114, 2018.
- [52] J. Qiao, X. Shen, J. W. Mark, and Y. He. Mac-layer concurrent beamforming protocol for indoor millimeter-wave networks. *IEEE Transactions on Vehicular Technology*, 64(1):327–338, 2014.
- [53] Qualcomm. Linux wil6210 driver. <https://github.com/torvalds/linux/tree/master/drivers/net/wireless/ath/wil6210>, Aug. 2017.
- [54] T. S. Rappaport, E. Ben-Dor, J. N. Murdock, and Y. Qiao. 38 GHz and 60 GHz angle-dependent propagation for cellular & peer-to-peer wireless communications. In

2012 IEEE international conference on communications (ICC), pages 4568–4573. IEEE, 2012.

[55] T. S. Rappaport et al. Millimeter wave mobile communications for 5G cellular: It will work! *IEEE Access*, 1:335–349, May 2013.

[56] T. S. Rappaport, F. Gutierrez, E. Ben-Dor, J. N. Murdock, Y. Qiao, and J. I. Tamir. Broadband millimeter-wave propagation measurements and models using adaptive-beam antennas for outdoor urban cellular communications. *IEEE transactions on antennas and propagation*, 61(4):1850–1859, 2012.

[57] M. E. Rasekh, Z. Marzi, Y. Zhu, U. Madhow, and H. Zheng. Noncoherent mmwave path tracking. In *Proceedings of the 18th International Workshop on Mobile Computing Systems and Applications*, pages 13–18, 2017.

[58] V. V. Ratnam and A. F. Molisch. Continuous analog channel estimation-aided beamforming for Massive MIMO systems. *IEEE Transactions on Wireless Communications*, 18(12):5557–5570, 2019.

[59] D. Raychaudhuri, I. Seskar, G. Zussman, T. Korakis, D. Kilper, T. Chen, J. Kolodziejski, M. Sherman, Z. Kostic, X. Gu, et al. Challenge: COSMOS: A city-scale programmable testbed for experimentation with advanced wireless. In *Proceedings of the 26th Annual International Conference on Mobile Computing and Networking*, pages 1–13, 2020.

[60] Remcom. Wireless Insite 3D Wireless Prediction Software. <https://www.remcom.com/wireless-insite-em-propagation-software>, 2020.

[61] B. Sadhu, A. Paidimarri, M. Ferriss, M. Yeck, X. Gu, and A. Valdes-Garcia. A 128-element dual-polarized software-defined phased array radio for mm-wave 5G experimentation. In *Proceedings of the 2nd ACM Workshop on Millimeter Wave Networks and Sensing Systems*, pages 21–25, 2018.

[62] Samsung. Samsung 5G phased array. <http://bit.ly/2oNSbnx>, 2020.

[63] A. M. Sayeed and V. Raghavan. Maximizing MIMO capacity in sparse multipath with reconfigurable antenna arrays. *IEEE Journal of Selected Topics in Signal Processing*, 1(1):156–166, 2007.

[64] S. Shao, H. Zhang, D. Koutsonikolas, and A. Khreishah. Two-dimensional reduction of beam training overhead in crowded 802.11 ad based networks. In *IEEE INFOCOM 2018-IEEE Conference on Computer Communications Workshops (INFOCOM WKSHPs)*, pages 680–685. IEEE, 2018.

[65] S. Sun and T. S. Rappaport. Multi-beam antenna combining for 28 GHz cellular link improvement in urban environments. In *2013 IEEE Global Communications Conference (GLOBECOM)*, pages 3754–3759. IEEE, 2013.

[66] S. Sur, I. Pefkianakis, X. Zhang, and K.-H. Kim. WiFi-assisted 60 GHz wireless networks. In *Proceedings of the 23rd Annual International Conference on Mobile Computing and Networking*, pages 28–41. ACM, 2017.

[67] S. Sur, I. Pefkianakis, X. Zhang, and K.-H. Kim. Towards scalable and ubiquitous millimeter-wave wireless networks. In *Proceedings of the 24th Annual International Conference on Mobile Computing and Networking*, pages 257–271. ACM, 2018.

[68] S. Sur, V. Venkateswaran, X. Zhang, and P. Ramanathan. 60 GHz indoor networking through flexible beams: A link-level profiling. In *ACM SIGMETRICS Performance Evaluation Review*, volume 43, pages 71–84. ACM, 2015.

[69] S. Sur, X. Zhang, P. Ramanathan, and R. Chandra. Beamspy: enabling robust 60 GHz links under blockage. In *13th {USENIX} Symposium on Networked Systems Design and Implementation ({NSDI} 16)*, pages 193–206, 2016.

[70] X. Tan, Z. Sun, D. Koutsonikolas, and J. M. Jornet. Enabling indoor mobile millimeter-wave networks based on smart reflect-arrays. In *IEEE INFOCOM 2018-IEEE Conference on Computer Communications*, pages 270–278. IEEE, 2018.

[71] I. Telecom Infra Project. Analysis of 28GHz and 60GHz channel measurements in an indoor environment. <https://telecominfraproject.com/>, Aug. 2019.

[72] Y. M. Tsang, A. S. Poon, and S. Addepalli. Coding the beams: Improving beamforming training in mmwave communication system. In *Global Telecommunications Conference (GLOBECOM 2011)*, 2011 IEEE, pages 1–6. IEEE, 2011.

[73] D. Tse and P. Viswanath. *Fundamentals of wireless communication*. Cambridge university press, 2005.

[74] V. Va, X. Zhang, and R. W. Heath. Beam switching for millimeter wave communication to support high speed trains. In *2015 IEEE 82nd Vehicular Technology Conference (VTC2015-Fall)*, pages 1–5. IEEE, 2015.

[75] S. Wang, J. Huang, and X. Zhang. Demystifying millimeter-wave V2X: Towards robust and efficient directional connectivity under high mobility. In *Proceedings of the 26th Annual International Conference on Mobile Computing and Networking*, pages 1–14, 2020.

[76] T. Wei and X. Zhang. Pose information assisted 60 GHz networks: Towards seamless coverage and mobility support. In *Proceedings of the 23rd Annual International Conference on Mobile Computing and Networking*, pages 42–55. ACM, 2017.

[77] T. Wei, A. Zhou, and X. Zhang. Facilitating robust 60 GHz network deployment by sensing ambient reflectors. In *14th {USENIX} Symposium on Networked Systems Design and Implementation ({NSDI} 17)*, pages 213–226, 2017.

[78] D. Zhang, M. Garude, and P. H. Pathak. mmchoir: Exploiting joint transmissions for reliable 60GHz mmwave wans. In *Proceedings of the Eighteenth ACM International Symposium on Mobile Ad Hoc Networking and Computing*, pages 251–260. ACM, 2018.

[79] M. Zhao, D. Liu, and F. Yu. Improving the robustness of 60 GHz indoor connectivity by deployment of mirrors. In *2018 IEEE 29th Annual International Symposium on Personal, Indoor and Mobile Radio Communications (PIMRC)*, pages 188–193. IEEE, 2018.

[80] A. Zhou, L. Wu, S. Xu, H. Ma, T. Wei, and X. Zhang. Following the shadow: Agile 3-D beam-steering for 60 GHz wireless networks. In *IEEE INFOCOM 2018-IEEE Conference on Computer Communications*, pages 2375–2383. IEEE, 2018.

[81] A. Zhou, S. Xu, S. Wang, J. Huang, S. Yang, T. Wei, X. Zhang, and H. Ma. Robot navigation in radio beam space: Leveraging robotic intelligence for seamless mmwave network coverage. In *Proceedings of the Twentieth ACM International Symposium on Mobile Ad Hoc Networking and Computing*, pages 161–170. ACM, 2019.

[82] A. Zhou, S. Yang, Y. Yang, Y. Fan, and H. Ma. Autonomous environment mapping using commodity millimeter-wave network device. In *IEEE INFOCOM 2019-IEEE Conference on Computer Communications*, pages 1126–1134. IEEE, 2019.

[83] A. Zhou, X. Zhang, and H. Ma. Beam-forecast: Facilitating mobile 60 GHz networks via model-driven beam steering. In *IEEE INFOCOM 2017-IEEE Conference on Computer Communications*, pages 1–9. IEEE, 2017.

[84] L. Zhou and Y. Ohashi. Efficient codebook-based MIMO beamforming for millimeter-wave WLANs. In *Personal Indoor and Mobile Radio Communications (PIMRC), 2012 IEEE 23rd International Symposium on*, pages 1885–1889. IEEE, 2012.

[85] X. Zhou, Z. Zhang, Y. Zhu, Y. Li, S. Kumar, A. Vahdat, B. Y. Zhao, and H. Zheng. Mirror mirror on the ceiling: Flexible wireless links for data centers. *ACM SIGCOMM Computer Communication Review*, 42(4):443–454, 2012.

[86] Y. Zhu, Z. Zhang, Z. Marzi, C. Nelson, U. Madhow, B. Y. Zhao, and H. Zheng. Demystifying 60GHz outdoor picocells. In *Proceedings of the 20th annual international conference on Mobile computing and networking*, pages 5–16. ACM, 2014.

A HOW MULTI-BEAMS ARE OPTIMAL FOR SNR AND THROUGHPUT

Here we show that the multi-beam patterns with appropriate power and phase control are optimal such that they maximize the SNR at the receiver. To demonstrate the multi-beam optimality, we first construct the maximum likelihood (ML) based solution and then show that the multi-beam approaches the ML estimate. The transmit phased array applies beam weights \mathbf{w}_T to transmit signal $s[m]$ which then passes through channel \mathbf{h} . For simplicity, assume a single antenna at the receiver with a receive antenna gain of unity. The received signal $y[m]$ corrupted with noise $n[m]$ (m is symbol index) as follows:

$$y[m] = \mathbf{h}^T \mathbf{w}_T s[m] + n[m]. \quad (20)$$

We write the expression of SNR:

$$\text{SNR} = \frac{\|\mathbf{h}^T \mathbf{w}_T\|^2 P_T}{P_N}, \quad (21)$$

where $P_T = \sum_m \|x[m]\|^2$ is the average transmit power (without transmit antenna gain) and P_N is the noise power.

The optimal linear ML estimator for \mathbf{w}_T is given by

$$\begin{aligned} \hat{\mathbf{w}}_T &= \arg \max_{\mathbf{w}_T} \text{SNR} \\ \text{s.t. } \|\mathbf{w}_T\| &= 1, \end{aligned} \quad (22)$$

where the constraint $\|\mathbf{w}_T\| = 1$ normalizes the transmit beam pattern to satisfy the total radiated power constraint. The ML estimate of optimal beam weights is

$$\mathbf{w}_T^{\text{opt}} = \frac{\mathbf{h}^*}{\|\mathbf{h}\|}, \quad (23)$$

which provides the maximum SNR of $\frac{\|\mathbf{h}\|^2 P_T}{P_N}$ which is dependent on the multi-path channel taps.

We next show how it compares against the SNR of a single beam and our multi-beam system. We first write the channel in a geometric model representation [16, 63]:

$$\mathbf{h}(t) = \sum_{\ell=0}^{L-1} \mathbf{a}_T(\phi_\ell) \gamma_\ell e^{2\pi f_c \tau_\ell} \delta(t - \tau_\ell), \quad (24)$$

where we assume the channel is bounded by L paths and $\phi_\ell, \gamma_\ell, \tau_\ell$ represents the AoD, attenuation, and ToF of the ℓ^{th} path, respectively. The steering vector $\mathbf{a}_T(\phi_\ell)$ represents the relative phase shift introduced by each path at every antenna element (out of N_T elements) as $\mathbf{a}_T(\phi_\ell) = [1, e^{-j2\pi \frac{d}{\lambda} \sin(\phi_\ell)}, \dots, e^{-j2\pi(N_T-1) \frac{d}{\lambda} \sin(\phi_\ell)}]^T$

In the frequency domain, the channel is written at subcarrier k as follow:

$$\mathbf{h}(k) = \sum_{\ell=0}^{L-1} \mathbf{a}_T(\phi_\ell) \gamma_\ell e^{j2\pi(f_c + k\Delta f)\tau_\ell} \quad (25)$$

where f_c is center frequency and Δf is the subcarrier spacing.

The traditional single-beam pattern ignores the multi-path and creates a directional pattern along the strongest path (LOS or one of the reflectors). Assuming ϕ_0 is the direction of the strongest path, the single-beam antenna weights follows:

$$\begin{aligned} \mathbf{w}_T^{\text{single}} &= \mathbf{a}_T^*(\phi_0) / \|\mathbf{a}_T(\phi_0)\| \\ &= \frac{1}{\sqrt{N_T}} [1, e^{j2\pi \frac{d}{\lambda} \sin(\phi_0)}, \dots, e^{j2\pi(N-1) \frac{d}{\lambda} \sin(\phi_0)}]^T. \end{aligned} \quad (26)$$

Assuming a directional single-beam pattern severely attenuates other channel paths, the single-beam SNR consists only of the strongest path as:

$$\text{SNR}^{\text{single}} = \frac{\|\gamma_0\|^2 P_T}{P_N}. \quad (27)$$

Instead, we design phase-coherent multi-beam patterns which exploits B channel directions out of L paths as follow:

$$\mathbf{w}_T^{\text{multi}} = \frac{\sum_{b=0}^{B-1} \mathbf{a}_T^*(\phi_b) \gamma_b e^{j\zeta_b}}{\|\sum_{b=0}^{B-1} \mathbf{a}_T^*(\phi_b) \gamma_b e^{j\zeta_b}\|}, \quad (28)$$

where we orient all the B beams in the multi-beam along the B strongest paths in the channel. Note that our multi-beam patterns ensures that per-beam amplitude γ_b and phase ζ_b (averaged over all frequency subcarriers) is aligned with per-path channel attenuation and phase respectively. We clearly see that when $B = L$, i.e., the multi-beam patterns are oriented along all the paths in a multi-path channel. In this case, the multi-beam weights are same as the optimal weights in (23):

$$\mathbf{w}_T^{\text{multi}} = \mathbf{w}_T^{\text{opt}}, \quad \text{when } B = L. \quad (29)$$

Thus, a multi-beam pattern utilizes B out of L channel paths to improve the SNR as follows:

$$\text{SNR}^{\text{multi}} = \frac{\sum_{b=0}^{B-1} \|\gamma_b\|^2 P_T}{P_N}, \quad (30)$$

which converges to optimal SNR for $B = L$. The optimal ML beamformer requires per-antenna channel estimate which has a high complexity in terms of beam probing overhead [48]. *Since mmWave*

channel is sparse and there are only 1 or 2 strong reflected paths in addition to the direct path, the multi-beam with 2-3 beams provides SNR gain comparable to the optimal beam with significantly lower overhead.

B APPENDIX: MULTI-BEAM CHANNEL MODEL FOR TRACKING

We model multi-path channel and represent received signal strength as a function of known beamforming weights for a wideband system. Consider the transmitted signal $s[m]$ is loaded with analog phase shifts and attenuation through a complex weight vector \mathbf{w}_T as follows:

$$\mathbf{x}[m] = \mathbf{w}_T s[m] \quad (31)$$

The signal $\mathbf{x}[m]$ is attenuated by channel \mathbf{H} and then passed through complex weight vector \mathbf{w}_R at the receiver phased array, resulting in the received signal $y[m]$:

$$\begin{aligned} y[m] &= \mathbf{w}_R^H \mathbf{H} \mathbf{x}[m] + \mathbf{w}_R^H \mathbf{n}[m] \\ &= \mathbf{w}_R^H \mathbf{H} \mathbf{w}_T s[m] + \mathbf{w}_R^H \mathbf{n}[m], \end{aligned} \quad (32)$$

where where $(\cdot)^H$ is the Hermitian operator, \mathbf{H} is channel matrix of dimension $N_R \times N_T$ and $\mathbf{n}[m]$ represents $N_R \times 1$ Gaussian noise at the receiver; N_R and N_T are number of receive and transmit antennas respectively. The design of beam weights \mathbf{w}_T and \mathbf{w}_R to create multi-lobe beam patterns will be discussed in the next sub-section. We represent the effective channel experienced by the transmit signal as follows:

$$h_{\text{eff}} = \mathbf{w}_R^H \mathbf{H} \mathbf{w}_T. \quad (33)$$

To understand how the effective channel is related to the AoA (θ_ℓ), AoD (ϕ_ℓ), and ToF (τ_ℓ) of $l = 1, \dots, L$ dominant paths, we represent the channel using a geometric channel model which is widely used at mmWave frequencies [16, 63].

$$\begin{aligned} h_{\text{eff}} &= \sum_{\ell} \mathbf{w}_R^H \mathbf{a}_R(\theta_\ell) \mathbf{a}_T(\phi_\ell)^H \mathbf{w}_T \gamma_\ell e^{j2\pi f_c \tau_\ell} \delta(t - \tau_\ell) \\ &= \sum_{\ell} \alpha_\ell \delta(t - \tau_\ell), \end{aligned} \quad (34)$$

where $\mathbf{a}_R(\theta_\ell) = [1, e^{-j2\pi \frac{d}{\lambda} \sin(\theta_\ell)}, \dots, e^{-j2\pi(N_R-1) \frac{d}{\lambda} \sin(\theta_\ell)}]$ is the steering vector that represents the relative phase shift at each antennas experienced by the received signal appearing at an angle θ_ℓ to the received phased array; $\mathbf{a}_T(\phi_\ell)$ is defined similarly at the transmit array. The multi-path channel is represented by complex attenuation γ_ℓ and delay τ_ℓ along the ℓ^{th} path. From (17), we extract per-path power as

$$P_\ell = \|\mathbf{w}_R^H \mathbf{a}_R(\theta_\ell)\|^2 \|\mathbf{a}_T(\phi_\ell)^H \mathbf{w}_T\|^2 \|\gamma_\ell\|^2, \quad (35)$$

which we express in dB as

$$P_\ell \text{ (dB)} = G_R(\theta_\ell) + G_T(\phi_\ell) - P_h \text{ (in dB)}, \quad (36)$$

where $G_R(\theta_\ell)$, $G_T(\phi_\ell)$, and P_h denote the receive/transmit antenna gain and channel loss respectively. We make an important observation from (35) and (36) that the per-path power is a quadratic function of beamforming weights \mathbf{w}_R and \mathbf{w}_T which verifies the underlying ambiguity in the tracking algorithm as we discussed in Section 5.